UNIVERSITÄT
BERN

Graduate School for Cellular and Biomedical Sciences

University of Bern

Multidisciplinary Approaches toward an Improved Efficacy of Cochlear Implants

PhD Thesis submitted by

Wilhelm Wimmer

from **Austria**

for the degree of

PhD in Biomedical Engineering

Supervisor
Prof. Dr. Dr. Martin Kompis
Department of Otolaryngology, Head and Neck Surgery, Inselspital
Faculty of Medicine of the University of Bern

Co-advisor
PD Dr. Jürgen Burger
Institute for Surgical Technology and Biomechanics
Faculty of Medicine of the University of Bern

Accepted by the Faculty of Medicine, the Faculty of Science and the Vetsuisse Faculty of the University of Bern at the request of the Graduate School for Cellular and Biomedical Sciences

Bern, Dean of the Faculty of Medicine

Bern, Dean of the Faculty of Science

Bern, Dean of the Vetsuisse Faculty Bern

ACKNOWLEDGMENTS

This dissertation covers parts of the work conducted in the last 3 years at the ARTORG Center and the Inselspital in Bern, Switzerland. During this time, I was allowed to collaborate with many exciting persons, without whom it would not have been possible to complete this thesis.

First of all, I would like to thank the persons that gave me the opportunity to undertake a PhD in an area that has been always fascinating to me. My PhD supervisor, Prof. Martin Kompis, for guiding the thesis and for sharing his ideas and expertise in the field of audiology; Prof. Stefan Weber, for his way of challenging clinical problems and providing visions, and for encouraging me throughout the thesis; and, Prof. Marco Caversaccio, for giving a comprehensive insight into otology, and for his motivation and great support right from the beginning. I would also like to thank the members of my PhD expert committee: Prof. Jürgen Burger and Prof. Philippe Zysset, for co-advising and mentoring the work of the last years; my sincere thanks go to Prof. Norbert Dillier, who agreed to review this thesis on a very short notice.

The work presented herein is the result of many collaborations. I want to particularly thank our clinical partners at the Inselspital; the team in the audiology department, for their assistance: Beatrix Richard, Cilly Huber, Julia Bernath, Lilian Tschan, Sandra Schenk, Benjamin von Gunten, Christoph Schmid, and Thomas Wieland. Special thanks go to Martin Krebs, who taught me a lot and always helped me with administrative tasks. Furthermore, I want to to thank the teams of the ENT clinic and neuroradiology for their priceless support, especially Jacqueline Diethelm, Susanne Hofmann, Bernd Werle, Krzysztof Szmigiel, Mamdouh Nogdalla, Theo Hofmann, and Nexi Avdija.

In addition, I want to thank our collaborating surgeons from the ENT clinic: Dr. Cilga Dür, Dr. Andreas Arnold, Dr. Georgios Mantokoudis, Dr. Markus Huth, Dr. Pascal Senn, Dr. Patrick Dubach, and Dr. Stefan Weder. Special thanks go to Nane Boemke from the Institute of Anatomy, for her irreplaceable dedication and assistance.

I wish to thank our collaborators from the University Hospital Montpellier, France: Prof. Alain Uziel, Prof. Frederic Venail, and Dr. Mohamed Akkari. I would also like to thank the Nano-Tera funding initiative, as well as our industrial collaborators from Med-El, Oticon Medical, and Scanco Medical, for their in-kind or financial support.

Many thanks go to my current and former colleagues at the ARTORG center, for making this place unique and for their great help: Anja Kurz, Denise Baumann, Diana Kleinert, Madeleine Steiger, Kate Gerber, Alex Juarez, Christoph Rathgeb, Dawei Chen, Giuseppe Zito, Jeremie Guignard, Jonas Salzmann, Juan Anso, Manuel Stebinger, Marco Matulic, Marius Schwalbe, Matteo Fusaglia, Sandro De Zanet, Stefanos Apostolopoulos, and Tom Williamson. Many of the mentioned people show not only interests in science, but also in enjoying a beer after work.

Finally, I would like to thank my family: my parents Wahiba and Wilhelm, and my sisters Olivia, Caroline, and Sophie Marie, for their love and overwhelming support; my parents-in-law, Silvia and Guido, for making Bern a second home. Most importantly, I want to express my love and gratitude to my wife Selina, the reason why I came to Bern, for her support and love, for sharing her life with me, and for giving birth to our little Leila. We are proud and happy to have you with us!

ABSTRACT

The cochlear implant (CI) is an auditory prosthesis that electrically stimulates the cochlear nerve to restore hearing. Although modern CI systems have proven to be a successful treatment for hearing impaired or deaf people, there are significant differences in the performance between people with normal hearing and CI recipients. This thesis aims to contribute to the field of cochlear implantation with a multidisciplinary approach, addressing problems related to minimally invasive surgical implantation and front-end processing of CI audio processors.

First, concepts required for the clinical application of a minimally invasive robotic cochlear implantation approach were investigated. A computer-assisted method for scala tympani access and insertion trajectory planning was developed and evaluated in ex vivo models. With the proposed method, it was possible to achieve full scala tympani insertions in cases demanding a trajectory positioning accuracy below 0.5 mm. The study demonstrated that an optimal access to the scala tympani can be planned and performed with the robotic system. Furthermore, a manual insertion procedure for the minimally invasive approach was developed and tested. In all 8 tested specimens it was possible to insert the CI electrode arrays through the small drill tunnel using the proposed procedure, showing the feasibility of the approach.

Second, front-end processing strategies of novel CI audio processors were evaluated. The influence of the microphone position of a single-unit processor on speech intelligibility in noise was investigated in a clinical study with 12 experienced CI users. It was shown that detrimental effects on speech reception are introduced by microphones positioned further to the back of the head. The signal-to-noise ratio was significantly better with the behind-the-ear processor when compared with the single-unit processor, if noise was presented from behind (4.4 dB, $p < 0.001$). Directional microphone systems could be applied to overcome this drawback. A second audiological study with 10 subjects evaluated the expected benefit of a pinna effect imitating directional microphone system. The directional microphone setting

improved the speech reception thresholds by up to 3.6 dB ($p < 0.01$) on average when compared to the omnidirectional mode, indicating that CI users can benefit from the directional microphone system.

CONTENTS

LIST OF ACRONYMS

CBCT	Cone beam computed tomography
CI	Cochlear implant
CIS	Continuous interleaved sampling
CROS	Contralateral routing of signal
DCA	Direct cochlear access
EABR	Electrically evoked auditory brainstem responses
EAC	External auditory canal
EAS	Electric acoustic stimulation
ECAP	Electrically evoked compound action potentials
ESRT	Electrically evoked stapedial reflexes
HL	Hearing level
MicroCT	Micro-computed tomography
RW	Round window
SM	Scala media
SNR	Signal-to-noise ratio
SPL	Sound pressure level
SRT	Speech reception threshold
SSD	Single-sided deafness
ST	Scala tympani
SV	Scala vestibuli

CHAPTER 1

INTRODUCTION

A short introduction to the anatomy and physiology of the human ear is provided and the different types of peripheral hearing loss and therapies are described. Particular emphasis is placed on cochlear implants, their design and function, and the clinical aspects of cochlear implantation. An overview of current deficits of cochlear implants is given and the objectives of the thesis are described.

1.1 Motivation

In 2012, a report of the World Health Organization (WHO) identified hearing impairment as one of the most prevalent chronic disabilities in the world and estimated about 360 million persons to suffer from disabling hearing loss [1]. While mild hearing loss can cause communication difficulties, especially in background noise, the impact of more severe forms of hearing impairment is further-reaching. Hearing is critical to language development in the first years of a child's life, and pediatric hearing loss is known to negatively influence the educational and psychosocial development [2]. In adults, untreated hearing loss can have detrimental social, psychological, cognitive, and health-associated consequences, and may lead to isolation and withdrawal [3].

Among the multitude of available treatment modalities for hearing impairment, the cochlear implant (CI) can be considered the most outstanding technical achievement of the last decades [4]. The CI is an auditory prosthesis that is able to restore the hearing sense of hearing impaired or even completely deaf people. Currently available CIs are highly complex and well-advanced systems that systematically demonstrated to be a successful treatment option. However, a high variability in therapy outcome remains persistent and CI recipients still experience difficulties with speech reception in crowded or noisy settings. To a certain degree these issues can be associated with the technical limitations of modern CI systems. Therefore, to improve the efficacy of current implant systems, this thesis applies a multidisciplinary approach that covers concepts of otology, audiology, and computational engineering. Specifically, issues related to minimally invasive cochlear implantation and CI front-end technology are addressed.

In the following sections, the human ear anatomy, physiology, and pathology are briefly summarized to provide the background knowledge required for an understanding of current CI technology and concepts, and the deficits examined in this thesis.

1.2 Anatomy and Physiology of the Human Ear

The human ear can be anatomically and functionally divided into 3 parts: the outer ear, the middle ear and the inner ear (Fig. 1.1). The ear is the peripheral part of the auditory system and transduces sound pressure waves into neural action potentials. These signals are transmitted through the cochlear nerve and further processed in the central auditory system, ultimately leading to the perception of sound.

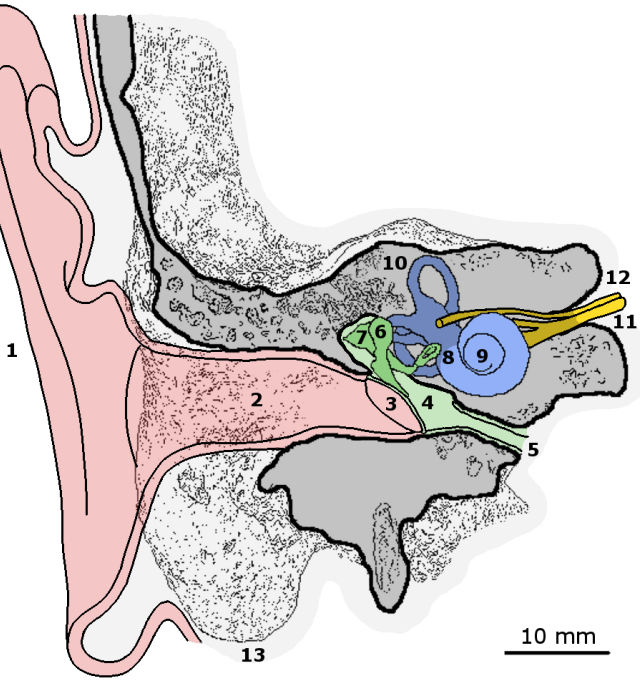

Fig. 1.1. Coronal section of a right temporal bone showing the outer ear (shaded red), the middle ear (shaded green), and the inner ear (shaded blue); anterior view. Pinna (1); external auditory canal (2); tympanic membrane (3); tympanic cavity (4); Eustachian tube (5); malleus (6); incus (7); stapes and oval window (8); cochlea (9); semicircular canals (10); vestibulocochlear nerve (11); facial nerve (12); mastoid tip (13). *Image based on computed tomography data.*

Outer ear

The outer ear consists of the pinna and the external auditory canal (EAC). It collects and directs sound pressure waves from the free sound field to the tympanic membrane. The shape of the outer ear acts as a frequency-selective directional filter (pinna effect). Signal components in the frequency range between 1.5 and 7 kHz are amplified [5–7]. The pinna has a stronger directionality to the front at frequencies higher than 2 kHz [8]. It plays an important role in spatial hearing, because it encodes the direction of sound incidence in the signal spectrum. These so-called monaural cues enable sound localization in the median plane and reduce the occurrence of front-back confusions [9, 10].

Middle ear

The tympanic membrane separates the outer ear from the middle ear, an air-filled space (tympanic cavity) that contains the ossicles, the middle ear muscles and a portion of the chorda tympani. The ossicles (malleus, incus, and stapes) transfer the vibrations at the tympanic membrane to the oval window of the cochlea. At the same time the pressure amplitude is amplified approximately by a factor of 22, reducing the impedance mismatch between the outer ear and the fluid-filled inner ear, and allowing an efficient sound transmission [11, 12].

The tympanic cavity communicates with the nasopharynx through the Eustachian tube, enabling air pressure equalization between both sides of the tympanic membrane. The physiological role of the middle ear muscles (m. tensor tympani and m. stapedius) is not completely understood, probable functions are the attenuation of low-frequency noise (below 2 kHz), the protection against permanent damage to the inner ear caused by loud sounds, and the attenuation of self-generated sounds, such as one's own speech [13–15].

Inner ear

The inner ear is located in the petrous portion of the temporal bone. It contains 2 fluid-filled partitions: the bony and the membranous labyrinth. The bony labyrinth is composed of the cavities of the cochlea, the vestibule, and the semicircular canals and is filled with

perilymph. The endolymph containing membranous labyrinth lies within the bony labyrinth.

The auditory part of the inner ear is the cochlea, a helical structure with an average length of 35 mm and approximately $2^3/_4$ turns. Remarkably, an extensive anatomic variation in dimension and shape can be observed in humans, with cochlear duct lengths ranging from 25 to 45 mm [16–19]. Figure 1.2 shows a cross section of a cochlea based on micro-computed tomography (MicroCT) images. Three separated compartments can be identified in each turn of the cochlear channel: the scala media (SM), the scala tympani (ST), and the scala vestibuli (SV). The SM (or cochlear duct) ends at the cochlear apex and is separated from the perilymphatic space by the basilar membrane and Reissner's membrane (see Figure 1.3). The receptor organ of hearing, the organ of Corti, sits on the basilar membrane and coils along the entire length of the cochlea. It is a complex compound of supporting structures and 2 types of sensory cells, the inner and outer hair cells. The inner hair cells are arranged in a single row, while the outer hair cells occur in 3 to 5 rows. In a human cochlea about 3,500 inner and 12,000 outer hair cells can be found. The

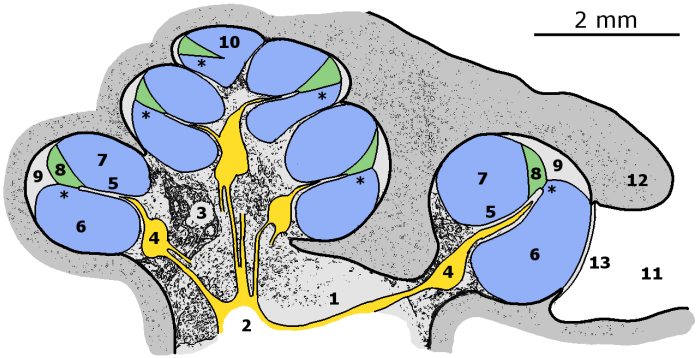

Fig. 1.2. Axial section of a left human cochlea; inferior view. Internal auditory canal (1); cochlear nerve (2); modiolus (3); spiral ganglion (4); osseous spiral lamina (5); scala tympani (6); scala vestibuli (7); scala media (8); spiral ligament (9); helicotrema (10); round window niche (11) and bony overhang (12); round window membrane (13). The position of the basilar membrane is indicated by asterisks. The other structures of the cochlear canal are marked in the basal turn only. The fluid-filled compartments are shaded blue (perilymph) and green (endolymph).

outer hair cells are attached to a jelly-like extracellular matrix, the tectorial membrane [20, 21]. It remains unclear whether the inner hair cells are directly linked to the tectorial membrane as well [17].

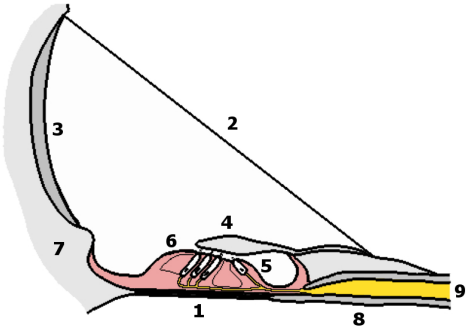

Fig. 1.3. Cross section of the scala media and the organ of Corti (shaded red). Basilar membrane (1); Reissner's membrane (2); stria vascularis (3); tectorial membrane (4); inner hair cell (5); outer hair cells (6); spiral ligament (7); osseous spiral lamina (8); spiral ganglion fibers (9). *Figure based on histological image.*

The footplate of the stapes is connected to the SV at the oval window. The ST and SV join at the helicotrema and the ST is terminated against the tympanic cavity at the round window (RW) membrane. Pressure changes at the oval window generate fluid motions that travel down the cochlea and result in a vibration of the basilar membrane. The mechanical properties of the basilar membrane vary considerably along the spiral: at the base it is narrow (100 μm) and stiff, and at the apex it is wider (500 μm) and more compliant [17, 22]. As a consequence, the position of the maximum displacement amplitude on the basilar membrane is frequency-dependent. Lower frequencies are resonating toward the helicotrema and higher frequencies closer to the oval window (tonotopy) [12, 23]. The contractible outer hair cells serve as active non-linear amplifiers of the basilar membrane motion for input levels until 50 dB hearing level (HL) and increase the frequency discrimination [24]. The inner hair cells are considered the principle site of sound reception. The movement of the basilar membrane with respect to the tectorial membrane causes a displacement of the inner hair cells and the generation of neural action potentials in the adjacent spiral ganglion nerve cells [25].

1.3 Peripheral Hearing Loss and Therapies

Many of the above mentioned anatomical structures can be affected by malfunctions leading to hearing impairment. Hearing disorders are categorized by the location of the compromised part in the auditory pathway. Peripheral hearing impairment can be of a conductive or sensorineural kind, a combination of both types in the same ear is called mixed hearing loss. In addition, central hearing disorders which affect the auditory processing in the central nervous system can be differentiated. A common classification of the severity of hearing loss used in German speaking countries is shown in Table 1.1 [11].

Table 1.1. Overview of hearing loss degrees [11].

Degree of hearing loss	PTA, dB HL
Normal hearing	0 to 20
Mild	20 to 40
Moderate	40 to 55
Moderately severe	55 to 70
Severe	70 to 90
Profound	above 90

PTA = Pure tone average at 0.5/1/2/4 kHz.

Conductive Hearing Loss

Conductive hearing loss is caused by an impaired sound transmission from the outer ear to the inner ear, resulting in an attenuated sound intensity arriving at the cochlea. Common causes include the absence or blockage of the EAC (e.g., atresia or cerumen obturans), tympanic membrane perforation, a fluid-filled tympanic cavity (middle ear infections), and limited mobility of the ossicles (e.g., otosclerosis) [11].

Treatment modalities for conductive hearing loss include pharmaceutical as well as surgical measures and/or the provision of hearing aids. Depending on the audiological and otological findings, conventional hearing aids, bone conduction devices or implants [26, 27], or middle ear implants can be the best choice for the the patient [28].

Sensorineural Hearing Loss

Sensorineural hearing loss occurs if the structures of the inner ear (cochlear hearing loss) or, much less frequently, the cochlear nerve or synapses (auditory neuropathy/synaptopathy, retrocochlear hearing loss) are malfunctioning or damaged. The most common causes for cochlear hearing loss are presbycusis (age-related hearing loss), acoustic trauma, inner ear disorders (e.g., Meniere's disease) and infections (e.g., meningitis), genetic causes, ototoxic drugs, and sudden deafness [29]. As opposed to a pure conductive hearing impairment, patients with cochlear hearing loss face challenges that cannot be overcome by linear acoustic amplification. In particular, the speech intelligibility is impaired because of a distortion of the incoming acoustic signal. Furthermore, they experience a reduced audibility of soft sounds while higher sound intensities are still perceived as loud. This phenomenon is called recruitment and is believed to be caused by the loss of the cochlear amplification provided by the outer hair cells [11].

Today, conventional hearing aids are most often used as a treatment for mild to severe sensorineural hearing loss. If conventional hearing aids are contraindicated, middle ear implants are possible therapies [28]. In the case of sensorineural single-sided deafness (SSD), contralaterally placed conventional contralateral routing of signal (CROS) hearing aids or bone conduction implants can be used for treatment [30]. Less than 10% of hearing impaired patients present bilateral severe-to-profound hearing loss. The benefit of the aforementioned treatment options is very limited in this cohort, because insufficient information for adequate speech perception is provided through hearing aids. However, these patients can benefit from cochlear implants [31].

1.4 Cochlear Implants

The cochlear implant (CI) is an auditory prosthesis that bypasses non-functioning parts of the cochlea and directly stimulates the cochlear nerve with electrical impulses. In 1957, a French group achieved the first stimulation of the cochlear nerve with an implanted electrode [32]. Especially since the 1980s, the CI was further advanced from an experimental device to the predominant treatment for profound hearing loss [33]. To date, over 400,000 CIs have been implanted worldwide in patients with severe-to-profound deafness [34].

CI Design and Function

Current CI systems consist of an implantable part and an external audio processor (Fig. 1.4). The external part is usually worn behind

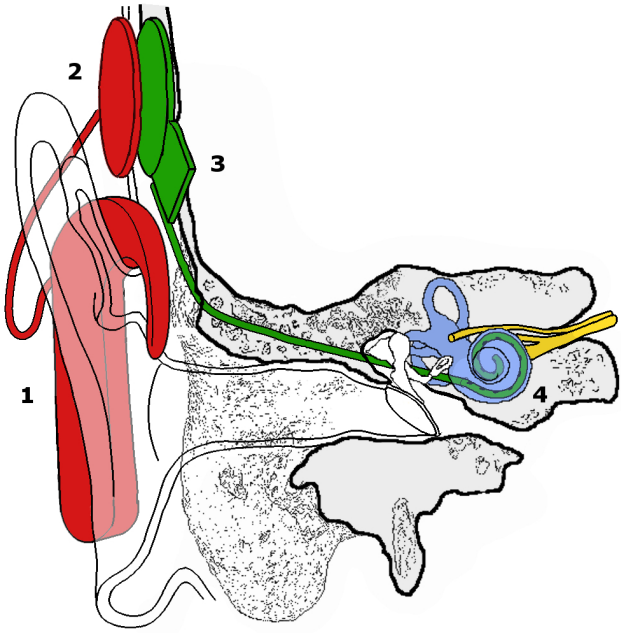

Fig. 1.4. The main parts of a cochlear implant system. External audio processor (1); transmission coil (2); implant with receiver/stimulator unit (3); inserted electrode array (4).

the ear and consists of one or more microphones, the batteries, the signal processing unit, and the transmission coil which is magnetically held above the implant. The implantable part consists of a receiving coil, the receiver/stimulator unit, the reference electrode which can be part of the implant body, and the electrode array that is inserted into the cochlea.

The audio processor records and processes incoming sound signals from the environment. Multiple microphone systems can be applied to improve the speech intelligibility in background noise (e.g., with directional microphone systems and signal enhancement strategies) [35, 36]. CI systems mimic the tonotopic stimulation present in the cochlea and mainly use signal processing methods based on the continuous interleaved sampling (CIS) speech coding strategy [37]. The signal processing chain involves a stage (so-called automatic gain control) to compress the dynamic range of acoustic signals (up to about 100 dB) to a range applicable for digital processing. Subsequently, the signal is band-pass filtered to assign the spectral information to the corresponding stimulation channel. In each channel, the signal envelope is extracted to modulate the amplitude of stimulation pulse trains. A logarithmic function is used to map the stimulation current to the recipient's electrical dynamic range. This range is much smaller than the acoustic dynamic range of a healthy ear and varies largely between individuals (between 5 to 20 dB). The stimuli are sent to one electrode after the other at rates that can reach up to 5,000 pulses per second [38]. Usually the stimulation patterns are applied through biphasic pulses in a monopolar electrode configuration [31]. Today, the most commonly used coding strategies in commercial systems are enhancements of the CIS strategy and aim to improve the sound perception through channel-selective algorithms (ACE and MP3000), current-steered stimuli to generate virtual channels (HiRes Fidelity 120), or variable stimulation rates at apical electrodes for temporal fine structure information (FSP) [39–43].

The encoded signal is transcutaneously transmitted to the implant via a radio frequency link. The receiver/stimulator unit decodes the signal and generates the stimulation pattern for the electrode array. Modern electrode arrays have 12 to 22 electrodes and are available in different lengths, mainly to fit the surgical demands in patients with residual hearing and malformed cochleae [44, 45]. The useful maximum number of stimulation channels is primarily restricted by the channel interaction (spread of excitation). Studies

have shown that the contribution of more than 8 active electrodes to an improved speech intelligibility in quiet is limited [31, 46–48].

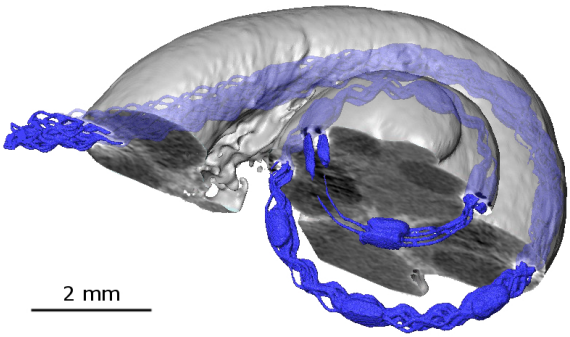

Fig. 1.5. 3D surface model of a left human cochlea with a deeply inserted free-fitting electrode array (blue). In this case, the array was inserted through the round window (approximately 2 turns). *Image rendered from MicroCT data.*

Different strategies regarding the intracochlear position of the array are pursued by researchers and CI manufacturers. Perimodiolar arrays are designed to self-coil around the modiolus to be placed adjacent to the spiral ganglion. Free-fitting arrays are more flexible and slide along the outer wall of the cochlea for a placement under the organ of Corti (Fig. 1.5). Potential advantages of electrodes positioned closer to the spiral ganglion such as decreased stimulation thresholds and better frequency discrimination were stated. However, no differences on the outcome of speech intelligibility or pitch detection have been shown so far [49–52], and the exact location of the excitation of cochlear neural structures through electrical pulses remains unclear [31, 48].

CI systems additionally provide a telemetry function to check the functional integrity of the implant, to measure the electrode impedances, and to record electrically evoked compound action potentials (ECAP) of the cochlear nerve, providing valuable information for later fitting of the CI.

Candidacy and Clinical Applications

The assessment of CI candidacy is a comprehensive process that involves radiological, medical, and audiological evaluations as well as psychological counselling. The primary indication is severe-to-profound bilateral sensorineural hearing loss with little or no benefit from conventional hearing aids. The best outcomes can be expected in postlingually deafened adults with a short duration of deafness and in early implanted prelingually deaf children. Poorer results can be expected in adults with prelingual deafness and a long duration of deafness [31]. Contraindications for CIs are an absent cochlea, some forms of severe cochlear malformations, a missing cochlear nerve, and a poor medical or psychological condition of the patient preventing surgery or participation in the speech-language therapy [11, 53].

The indication criteria for CIs are constantly expanding. As opposed to an unilateral CI treatment in patients with bilateral hearing loss, bilateral cochlear implantation enables the restoration of binaural hearing. Improved speech intelligibility in noise and sound localization have been demonstrated systematically in bilateral CI recipients [54–56].

Technical advancements of the implant design and the implantation technology have enabled to use CIs in patients with residual hearing. Systems with electric acoustic stimulation (EAS) combine the technology of CIs and hearing aids in the same ear. Lower frequencies are acoustically amplified, while higher frequencies are electrically stimulated over the inserted electrode array. If residual hearing is preserved, EAS users show significantly better speech understanding and spatial hearing abilities, and have a more natural music perception than can be expected with a normal CI [57–61].

Moreover, CIs are increasingly used as a treatment for single-sided deafness (SSD). Conventional CROS hearing aids and bone-conduction implants are well-established therapy options, because they reduce the head shadow effect and increase the responsiveness of the patients at the deaf ear side. Nevertheless, CIs additionally offer the potential advantages of binaural hearing, such as better speech understanding in noisy environments and improved spatial hearing abilities. Recent studies have reported on a successful rehabilitation of SSD with CIs, showing improved speech intelligibility in noise and sound localization. Nevertheless, further research is needed to refine the eligibility criteria, and sound localization still remains challenging for CI recipients with SSD [62–65].

The experiences found from CI patients have meanwhile shown promising results for tinnitus suppression. However, cochlear implantation can also cause tinnitus deterioration, and further investigations are necessary to understand the role of the CI as a treatment for tinnitus [66–68].

Cochlear Implantation

Today, cochlear implantation is a safe and worldwide routinely performed procedure. It is regularly carried out under general anesthesia and monitoring of the facial nerve function [69, 70]. Nevertheless, the complex anatomy of the temporal bone places high demands on the skills and experience of the surgeon. During the intervention 2 key stages can be identified. First, the surgeon needs to gain access to the cochlea. Second, the electrode array has to be inserted into the cochlea. In the following paragraphs, different techniques for cochlear implantation in non-malformed anatomy are briefly summarized.

Surgical Approaches

In the last decades, the transmastoid posterior tympanotomy (or facial recess) approach has become the standard procedure for cochlear access [71]. A cortical mastoidectomy is drilled to identify landmarks indicating the course of the facial nerve. Afterwards, a posterior tympanotomy is performed until the RW niche is sufficiently exposed [53, 72]. The size of the facial recess available for access to the RW niche is about 2 to 3 mm in adults and children at the level of the oval window [73]. If required, the chorda tympani can be sacrificed to extend the facial recess and increase the visibility of the cochlear promontory. Figure 1.6 illustrates a perspective view of the tympanic cavity and the facial recess. The cochlear promontory is directly exposed and an optimal insertion angle with respect to the basal turn of the cochlea is provided [74]. Cochlear implantation using a transmastoid posterior tympanotomy is considered safe, however, this approach needs experienced skills. Reports of facial nerve injury during implantation show a rate of less than 1%. Drawbacks of this approach are the need for a mastoidectomy and a sufficiently big facial recess [75].

For this reason, several alternative approaches have been elaborated in the past. Endoscopic techniques were developed for cochlear implantation to reduce the size of the mastoidectomy or to completely

avoid it. However, endoscopic interventions require a high training level of the surgeon for depth perception and orientation [76–78]. An alternative technique, the suprameatal approach, involves a tympanomeatal flap to visualize the tympanic cavity. A groove is prepared posterosuperior to the chorda tympani and connected with a tunnel drilled in the area superior to the EAC. During drilling, the facial nerve is protected by the incus. This approach avoids a mastoidectomy and posterior tympanotomy, nevertheless, it results in insertion angles 30 degrees superiorly compared to the facial recess approach [79, 80]. Furthermore, endaural implantation strategies have been developed. The Veria technique uses a custom designed tool to drill a canal to the tympanic cavity in the posterior wall of the EAC [81, 82]. In the pericanal approach, a rim is drilled into the posterosuperior region of the EAC to accommodate the electrode carrier [83]. The main disadvantages of the endaural techniques are the steep in-

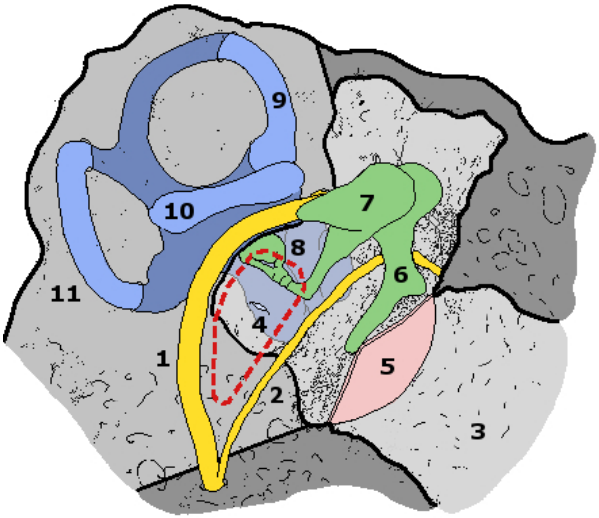

Fig. 1.6. Perspective view of the tympanic cavity and the facial recess (red dashed line); right temporal bone. During the intervention, the cochlear promontory is visible through the facial recess only. It is bound by the facial nerve (1), the chorda tympani (2), the fossa incudis (not shown), and the posterior wall (not shown) of the external auditory canal (3). Round window (4); tympanic membrane (5); malleus (6); incus (7); stapes (8); superior (9), lateral (10), and posterior semicircular canals (11). *Image based on computed-tomography data.*

sertion angle, the risk of tympanic membrane perforation, and the risk of electrode exposure and extrusion [75]. An opening of the middle ear is completely avoided with the middle fossa approach. The cochlea is accessed through a temporal craniotomy [84]. With this approach, patients are at elevated risk for postoperative complications, including meningitis, memory and speech disturbances, and a longer hospitalization [75].

Once the access to the tympanic cavity is established, the surgeon has to open the cochlea to insert the electrode array. For several reasons, the ST is the favored target for intracochlear array placement. It has larger dimensions than the SV and thus can better accommodate the electrode array [85, 86]. Furthermore, with an insertion into the SV the risk of damage to the fragile Reissner's membrane is higher [87]. Most importantly, speech intelligibility outcomes have shown to be better in CI recipients with ST insertions [88–91].

The surgeon can access the ST either directly through the RW, an extended RW, or a separately drilled cochleostomy. The optimal approach to the ST is a topic of discussion and closely relates to the type of the inserted electrode array [92–98]. The main advantages of an insertion through the RW are a safe placement within the ST and the prevention of drilling-induced damage to intracochlear structures. Furthermore, the RW membrane is a natural barrier against blood and bone dust [99]. The drawbacks of a strict RW approach are the steeper insertion angle at the first contact and the possibility of bending of the array in the hook region [94, 100]. In contrast, the extended RW and cochleostomy approaches (favorable for perimodiolar arrays) enable insertion vectors more tangentially to the course of the ST and provide an alternative access in malformed anatomy [74, 94, 96]. However, surgeons need to be experienced to find the correct drilling position and to keep the endosteum intact. To ensure an insertion into the ST, the cochleostomy should be performed inferior or anteroinferior to the RW [74, 87, 99–102].

Due to the tonotopic organization of the cochlea, the lower limit of frequencies available for stimulation is restricted by the the insertion depth of the electrode array [31]. The impact of the insertion depth on speech perception is rated differently by different authors [90, 103–107]. However, recent studies have shown that shallow insertions lead to bigger frequency mismatches with the default frequency allocations of CI systems [104, 108, 109].

Computer-Assisted Approaches

A different possibility to combine the advantages of the posterior tympanotomy approach (i.e., the optimized insertion angle) with the minimal invasiveness of alternative approaches is the utilization of computer-assisted technology. The first feasibility study of computer-navigated cochlear implantation in a cadaver specimen was presented in 2004 [110]. A reproducible target accuracy of 0.5 mm was defined as the requirement for systems applied in cochlear implantation. At that time, routinely used navigation systems did not meet this accuracy criterion. Consequently, computer-assisted methods were proposed to accomplish a minimally invasive keyhole approach for CI surgery. This approach, often referred to as percutaneous or direct cochlear access (DCA), avoids a mastoidectomy by drilling a small tunnel from the mastoid surface to the cochlea.

A concept for a DCA based on the principles of stereotactic surgery uses patient-specific drill guide templates [111]. The method involves the planning of a drilling trajectory on preoperative imaging data, the implantation of fixture pins in the temporal bone, additional imaging for patient-to-image registration, and the manufacturing of a patient-specific template with a milling machine. After the attachment of the template to the fixture pins, an otological drill is used to perform the DCA. In 2013, this approach was clinically tested in 8 patients showing 4 cases with complications related to electrode array insertion and 1 case of facial nerve paresis [112]. Concept-related issues, e.g., the lack of feedback information during the drilling procedure, limit the clinical applicability of this approach.

Other research groups investigated in robotic technology to achieve a minimally invasive DCA. Commercially available industrial robots were evaluated, however, the targeting accuracy demands of cochlear implantation were not reached [113, 114]. Further on, custom-developed robotic systems were proposed [115–117]. After years of successive improvements, the robotic system developed at the ARTORG Center, University of Bern achieved an overall target accuracy of 0.15 $\pm$ 0.08 mm (i.e., at the level of the RW) in 8 temporal bone specimens [118]. Figure 1.7 shows the system which comprises an optical tracking camera, a serial manipulator as well as a navigation platform and dedicated planning software [119, 120]. The robotic approach introduces major changes to the clinical procedure of cochlear implantation. The patient gets implanted with 4 small fiducial screws

under local anesthesia. After preoperative imaging, the DCA trajectory is planned by the surgeon and radiologist. The patient is registered to the plan with the fiducial screws and the robot automatically performs the DCA. The robotic system includes additional safety concepts, such as redundant force-based position estimation of the drill bit [121] and facial nerve monitoring [122], to avoid a blind drilling procedure. However, a clinically feasible implantation strategy after the completion of the DCA has to be developed prior to testing the system in a clinical study.

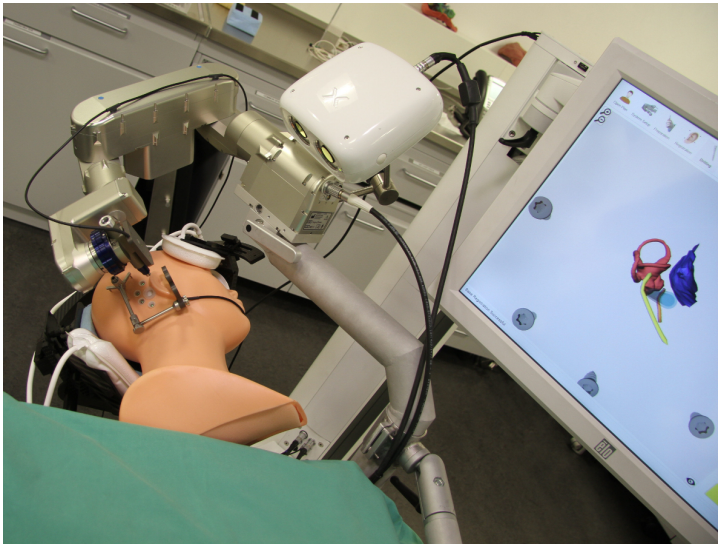

Fig. 1.7. The robotic system for a minimally invasive direct cochlear access developed in the ARTORG Center, University of Bern.

Processor Fitting and Rehabilitation Outcome

Typically a few weeks after the implantation, the external audio processor is programmed and activated for the first time. The electrode impedances are measured and non-effective or detrimental electrodes are deactivated (e.g., short/open circuits, extracochlear position, facial nerve stimulation). The maximum and minimum levels for the electrical stimulation are measured behaviorally, however, the recording of electrically evoked compound action potentials (ECAP) or

electrically evoked stapedial reflexes (ESRT) can be helpful. Further steps prior to microphone activation include channel-specific and overall loudness adjustments and balancing [123]. As CIs are auditory prostheses, the recipients have to learn to hear and to interpret new and at times unfamiliar sounds. This process involves additional follow-up sessions for a fitting refinement (regular sessions in the first months and later often at least 1 visit per year) and usually takes months of training together with speech therapists before an asymptotic level of speech perception is reached (usually after 3 to 6 months) [31].

Fig. 1.8. The multi-speaker setup for sound-field audiometry located in the ARTORG Center, University of Bern. The setup is primarily used for the preoperative and postoperative assessment of speech intelligibility in noise and spatial hearing abilities.

Different measurement methods can be used to evaluate the implant efficacy and treatment outcome after implantation. Objective measurements do not require the patient's cooperation, which is particularly important for small children. Clinically established methods for postoperative CI diagnostics include the measurements of ECAP, ESRT, and electrically evoked auditory brainstem responses (EABR) [11]. Subjective (or psychophysical) measurements depend on the feedback of the tested subject as a reaction to a given task. Dedicated questionnaires can be used to assess the subjective benefit (Quality of Life) including music perception and tinnitus [54, 124–127]. An integral component of the postoperative CI assessment is the sound-

field audiometry, which comprises the measurement of sound-field aided thresholds, speech audiometry, loudness scaling, and localization experiments. While CI recipients are able to achieve high speech recognition scores in a quiet environment, their speech intelligibility in noise remains impaired after the treatment [128]. Therefore, the evaluation of the speech intelligibility in noise is often an appropriate choice to quantify the benefit after cochlear implantation. These tests have to be performed in acoustic chambers and usually require measurement setups with multiple speakers (Fig. 1.8).

The postoperative benefit varies significantly between individual CI recipients and can range from a basic awareness of sound to open-set speech understanding and frequent telephone usage. The large individual differences in the postoperative outcome can be partially explained by patient-related and technology-related factors [4, 129]. Patient-related factors are associated with the individual etiology and medical history of the CI recipient. This can influence the condition and integrity of the peripheral and central auditory system at the time of implantation, such as the onset and/or duration of deafness or the extent of cochlear ossification [89, 130].

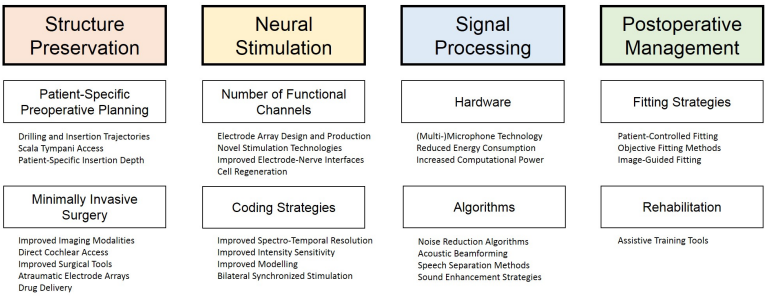

Fig. 1.9. An overview of current research areas and examples of technological aspects that can contribute to the efficacy of cochlear implant systems.

Besides the patient-related aspects, several technology-associated factors can be identified to influence the efficacy of a CI system. Figure 1.9 summarizes different technology-related aspects that affect the CI efficacy and shows specific examples for potential improvements.

The preservation of intracochlear structures plays an important role in cochlear implantation. To that end, computer-assisted methods offer valuable potential advantages for structure preservation [4]. Preoperatively obtained radiological data can be used to generate plans that either assist the surgeon in a conventional approach or to serve as a feed-in for navigation-controlled systems. Furthermore, minimally invasive robotic approaches could be used to perform a DCA that integrates patient-specific insertion targets and vectors to reduce the insertion friction forces. The preservation of residual hearing could further be increased by the design of novel atraumatic electrode arrays [131], the selection of patient-specific electrode array lengths [132], or the development of improved surgical tools, e.g., insertion force monitoring instruments [133]. Other aspects of structure preservation include the retention and regeneration of neural structures by direct application of medication through the implant [134, 135].

Another research area of particular interest is the advancement of the hardware and software of the external audio processor for an increased CI efficacy. Multimicrophone systems represent an effective way to facilitate speech understanding in noisy acoustic environments [128]. Furthermore, the implementation of novel sound enhancement and noise reduction algorithms are measures with high potential [136].

Both above mentioned research areas promise clinically relevant improvements on the efficacy of CI systems in the short and long-term perspective. Therefore, this thesis has objectives in both domains, as described in the following section.

1.5 Thesis Objectives and Overview

This thesis aims to improve the efficacy of current CI systems with a multidisciplinary approach that applies otological, audiological, and computational concepts in 2 research areas: the examination of minimally invasive surgical procedures for cochlear implantation, and the clinical evaluation of novel CI audio processors with regard to speech intelligibility in noise.

In the first part of this thesis, computer-assisted methods and minimally invasive implantation concepts are developed with the aim to improve the preservation of anatomical structures during cochlear implantation. The robotic DCA approach developed in Bern offers several potential advantages, such as a minimally invasive access to the tympanic cavity and the possibility for an optimized ST access. In **Chapter 2**, the development and evaluation of a computer-assisted planning method that considers the position and course of the ST is presented. The robotic system has shown to fulfill the accuracy demands required for a clinical application in cochlear implantation, however, aspects related to electrode array insertion remain to be addressed. The robotic approach introduces challenges to the insertion process of the CI array, mainly because the small tunnel (1.8 mm in diameter) is limiting the space available for electrode array control. In this context, the conception and validation of an insertion method applicable for the minimally invasive robotic approach is described in **Chapter 3**.

In the second part, the thesis turns to the area of front-end signal processing and focuses on the clinical evaluation of CI audio processors. The assessment of the speech in noise performance with novel designs and front-end processing technology may provide valuable information for the scientific and clinical community, e.g., for processor fitting or patient consultation. In **Chapter 4**, it is investigated how the wearing position of a single-unit audio processor, and thus its built-in omnidirectional microphone, affects speech reception in noise. In addition, computational and physical models are used to estimate the expected outcomes for the speech in noise experiments. Correspondingly, in **Chapter 5**, the speech in noise performance with a new directional microphone system that imitates the pinna effect is evaluated.

In the last chapter of the thesis, **Chapter 6**, the contributions and limitations of the presented research projects are discussed and an outlook on upcoming work is provided.

CHAPTER 2

COCHLEAR IMPLANT INSERTION TRAJECTORY AND SCALA TYMPANI ACCESS PLANNING

This chapter is published as:
Wimmer W, Venail F, Williamson T, Akkari M, Gerber N, Weber S, Caversaccio M, Uziel A, Bell B. Semiautomatic cochleostomy target and insertion trajectory planning for minimally invasive cochlear implantation. Biomed Res Int 2014; DOI: 10.1155/2014/596498.

The development and evaluation of a computer-assisted planning method for a minimally invasive scala tympani access is described. A landmark-based method is introduced and validated in a cadaver model. The results of the evaluation indicate that the method can be used to achieve safe scala tympani insertions.

2.1 Abstract

A major component of minimally invasive cochlear implantation is atraumatic scala tympani (ST) placement of the electrode array. This work reports on a semiautomatic planning paradigm that uses anatomical landmarks and cochlear surface models for cochleostomy target and insertion trajectory computation. The method was validated in a human whole head cadaver model (n = 10 temporal bones). Cochleostomy targets were generated from an automated script and used for consecutive planning of a direct cochlear access (DCA) drill trajectory from the mastoid surface to the inner ear. An image-guided robotic system was used to perform both, DCA and cochleostomy drilling. Nine of 10 implanted specimens showed complete ST placement. One case of scala vestibuli (SV) insertion occurred due to a registration/drilling error of 0.79 mm. The presented approach indicates that a safe cochleostomy target and insertion trajectory can be planned using conventional clinical imaging modalities, which lack sufficient resolution to identify the basilar membrane.

2.2 Introduction

The aims of minimally invasive cochlear implant (CI) surgery are manifold. On the one hand, minimally invasive access to the cochlea is gained through a DCA, which is a small tunnel drilled from the mastoid surface to the cochlea passing through the facial recess [112, 118]. In addition to a minimally invasive access, the preservation of intracochlear structures during and after electrode array insertion is an important research topic.

Once access to the tympanic cavity is established, the cochlea must be opened to enable CI electrode array insertion. Two criteria are primarily considered in the current definition of atraumatic electrode insertion. First, the ST is the favored intracochlear lumen for implant placement, especially in terms of retaining residual hearing [58, 90–92, 137]. Second, the ideal insertion trajectory should align with the center line of the ST to prevent damage to the basilar membrane, the modiolus, or the spiral ligament during insertion. The ST can be accessed either through a strict round window (RW) approach, a RW related cochleostomy, or a promontory cochleostomy separated from the RW. Drilling the cochleostomy in the correct location is one of the major challenges the surgeon faces during the surgery. The position is chosen intraoperatively according to the anatomical situation of the promontory (i.e., inferior or anteroinferior to the RW membrane) to avoid damage to basal intracochlear structures [17, 70, 96, 100, 102, 138, 139].

In this context, image-guided cochleostomy approaches have been investigated to aid the surgeon in determining the proper drill site, but, to our knowledge, no clinical data has been published [140, 141]. Correct planning of the cochleostomy site and insertion trajectory rely on an accurate representation of the anatomy during planning. However, clinically applicable imaging modalities do not provide sufficient imaging resolution for direct detection of the ST. The RW remains the only consistent anatomical landmark for preoperative/intraoperative ST access planning. Meshik et al. [74] analyzed insertion trajectories in cadaveric temporal bones using microcomputed tomography (MicroCT) imaging for ST visualization and subsequent centerline computation. An alternative approach utilizes active shape modeling for approximation of the position of the ST. The first report of a clinical implementation of this concept showed complete ST implantation in 6 of 8 patients with minor complications [112].

Anatomical variations play an important role in the planning and execution of any surgical procedure. For this reason, we hypothesize that an interactive method is most appropriate during the planning phase as this leaves the ultimate decision in the hands of the surgeon and avoids errors arising from automatic black box methods. Furthermore, we posit that the accuracy afforded by an image-guided robotic system can allow the surgeon to perform the cochleostomy with sufficient accuracy to reliably place the electrode within the ST. This work will present a semiautomatic planning method, which allows the user to plan the cochleostomy site and insertion trajectory compared to an idealized centerline approach [74]. The method was tested in a whole head cadaver model wherein the planned trajectory and cochleostomy site were drilled using an image-guided robot system.

2.3 Materials and Methods

Cochleostomy and Insertion Trajectory Computation

To obtain cochleostomy target positions and insertion trajectories, a semiautomatic landmark based approach was implemented. The method consists of three subsequences: manual landmark identification, surface model generation of the cochlea, and automatic cochleostomy and trajectory computation. Landmark identification and cochlear surface model generation were performed in a medical image analysis software (Amira 5, VSG, Burlington, MA, USA). Oblique coronal, axial, and sagittal slices were aligned to visualize the cochlea according to international consensus [142]. As landmarks, the center of the RW at the bony overhang (R), the basal center of the modiolus (C), the apical center of the modiolus (A), and the inner wall at 0 degree reference angle (I) were defined (Fig. 2.1). Further, the cochlea, the vestibule, and the semicircular canals were segmented using a region growing algorithm. Structure labels outside the bony labyrinth were manually removed and a 3D surface model was generated.

A Matlab script (The MathWorks Inc., Natick, MA, US) was implemented for automatic cochleostomy target and insertion trajectory computation. The coordinates of the previously found landmarks and the cochlear surface model serve as input for the algorithm. A local

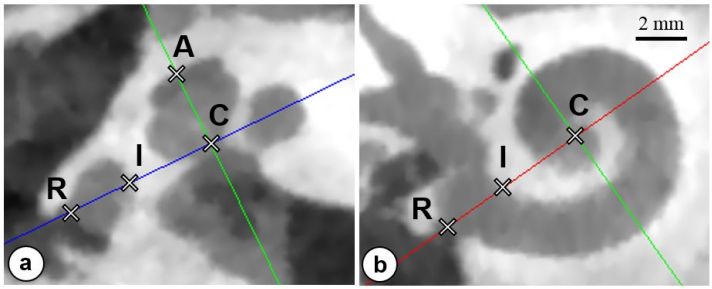

Fig. 2.1. Landmark identification of a right human cochlea using CBCT data. **a** Oblique axial slice corresponding to the 0 degree reference plane (red line in **b**, as defined in [142]). The RW center adjacent to the bony overhang (R), the inner wall border at the RW (I), the center of the modiolus in the basal turn (C), and the apical center of the modiolus (A) are used to define a local cochlear coordinate system for further computations. **b** Oblique coronal slice of the basal turn (blue line in **a**) and the corresponding in-plane landmark positions.

cochlear coordinate system based on cochlear landmarks is created (Fig. 2.2a). The origin of the coordinate system is placed in the basal center of the modiolus (C). The x-axis runs through the RW (landmark R), and the z-axis passes through the apical center of the modiolus (A). Finally, the y-axis is computed as the cross product of x and z. The cochlear model is simplified through 2 assumptions. First, the location of the basilar membrane is assumed to lie in the x-y plane in the basal turn of the cochlear model. Close to the RW membrane this assumption may not apply, since the basilar membrane orientates along the x-z plane [102]. Nevertheless, the simplification ensures that insertion trajectories are not oriented toward the basilar membrane in the basal turn. Additionally, it is supposed that the basilar membrane is not lying posterior to the x-y plane (i.e., negative z coordinates). The second major assumption is that the width of the ST in the region of interest does not exceed the distance between the landmarks R and I. The first stage of the algorithm involves the identification of surface points belonging to the ST. This is performed by truncating the set of points to those having positive y and negative z coordinates (Fig. 2.2a). Next, the algorithm removes points not belonging to the basal ST surface by satisfying the assumption that the ST width is no larger than the distance between R and I. The third step of the algorithm is the extraction of ST radial cross sections which are used to compute the ST centerline. This is accomplished by finding the nearest neighbor of a plane coincident with the z-axis with discrete angular steps (i.e., $\Delta\theta = 5°$; see Fig. 2.2b), starting at the RW ($\theta = 0°$) and extending throughout the first basal half turn ($\theta = 180°$). The center of gravity is calculated from the surface points in each cross section. Finally, a cubic spline is fit to the centers of gravity to approximate the mid-scala course of ST. An optimal insertion trajectory is defined as a line tangent to the smoothed spline at a defined basal turn angle θ. The corresponding cochleostomy points are found using a ray/triangle intersection algorithm [143]. The insertion trajectories and target points are computed in steps of 2 degrees up to a maximum of $\theta_C = 20°$ (Fig. 2.2c).

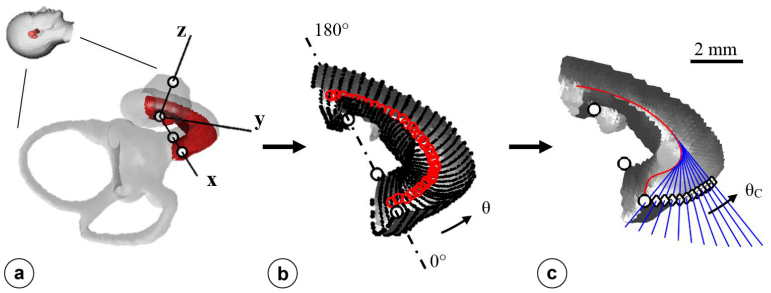

Fig. 2.2. Illustration of the automatic cochleostomy target/insertion trajectory computation algorithm. **a** Based on the landmarks (black circles), a local cochlear coordinate system is computed. As an assumption, the x-y plane is defined as the location of the basilar membrane. The surface model of the cochlea is truncated to the first half turn of the ST. **b** Radial cross sections are computed starting at the RW (0 degree reference).The center of gravity is estimated (red circles) based on the extracted vertices (black dots) for each cross section. **c** The centroid line (red line) is fitted with the data points, representing the mid-scala course of ST. For a specified range, the tangents of the centroid line are computed, defining the optimal insertion trajectories (blue lines) and the corresponding cochleostomy targets (diamonds) at the angular position θ_C.

Basilar Membrane Approximation Error

In order to verify that the assumptions for the approximation of the basilar membrane location apply, 5 datasets consisting of cone beam computed tomography (CBCT) and MicroCT images of human cochleae were used. Images of both modalities were registered and the displacement error between the actual position of the basilar membrane (MicroCT) and the approximated location (x-y plane, as found with the landmark based approach in CBCT) was assessed. An overall mean error of 0.23 mm was found for the first half of the basal turn. As expected, the error is higher close to the RW. In the region used for trajectory computation ($45° \leq \theta \leq 60°$), an average error of 0.22 mm was measured (Fig. 2.3).

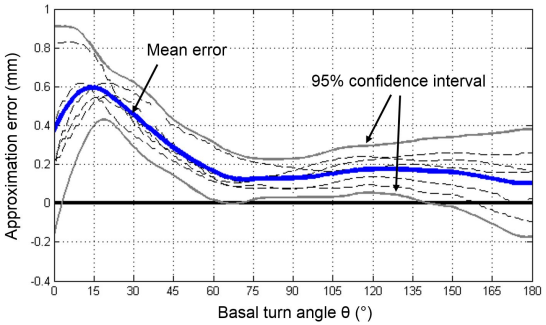

Fig. 2.3. The distance between the approximated position of the basilar membrane (as computed with the landmark based approach) and its actual position in the corresponding MicroCT data (blue line) of 5 human cochleae.

Ex Vivo Validation Study

Specimen Preparation and Preoperative Imaging

Five human cadaver heads (n = 10 temporal bones) fixed with 20% zinc chloride intra-arterial injection were used in this study. A minimally invasive access to the tympanic cavity was drilled with a purpose-built robotic system developed in Bern [118]. The system uses bone-anchored fiducial titanium screws for patient-to-image registration [120]. All experimental parts of the study (i.e., intervention planning, drilling, and array insertion) were performed in a laboratory of the University Hospital of Montpellier, France. High resolution CBCT scans (NewTom 5G, QR S.r.l, Verona, Italy) were acquired (voxel size: 125 µm isotropic, 110 kVp, 19 mA). For intraoperative endoscopic examination of the surgical procedure through the external auditory canal (EAC), the tympanic membrane was removed in all specimens.

Surgical Intervention Planning

The computed cochleostomy targets and trajectories, as well as the surface model of the cochlea, were imported into a dedicated surgical planning software [119]. The software allows the user to manually choose the drill/insertion trajectory based on the distances to critical structures in the temporal bone (i.e., facial nerve, chorda tympani, posterior wall of the EAC, and the ossicles) and in relation to the

computed ideal trajectory. In practice, the user defines a cochleostomy site (θ_C) and then adjusts the drill trajectory to minimize the deviation from the ideal. Two angular measures were introduced to facilitate this process [144]. First, the out of plane component is described by the angle δ. Second, the in-plane alignment is given by the angle ε as seen in Figure 2.4. Negative δ and ε values should be avoided as this indicates a collision with the basilar membrane and the modiolus, respectively. The final plan and alignment of the trajectory were performed by an experienced otolaryngologist with the goal of minimizing δ and ε.

DCA Drilling and Cochleostomy

The DCA tunnel was drilled using the same protocol published previously [118]. The DCA was drilled by the robot using a custom step drill having a proximal diameter of 2.5 mm with a length of 20 mm and distal portion with a diameter of 1.8 mm and a length of 10 mm to the tip. The drill motor was started (5,000 rpm) and the robot drilled with a feed rate of 0.5 mm/s using a pecking motion until the middle ear cavity was reached. A cochleostomy was then drilled (1 mm diamond burr) using the robot system. The drill speed was increased to 10,000 rpm, and the feed rate was reduced to 0.1 mm/s.

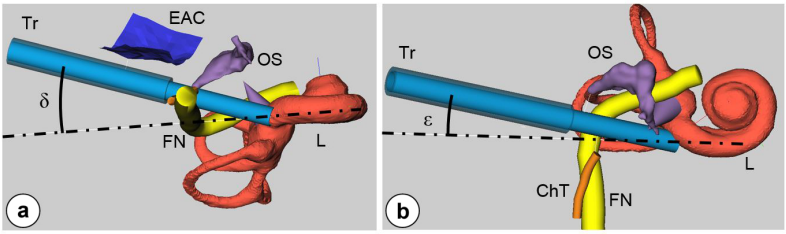

Fig. 2.4. Intervention planning for minimally invasive CI surgery in a dedicated software tool [119]. Visualization of the segmented posterior wall of the EAC, the facial nerve (FN), the chorda tympani (ChT), the ossicles (OS), and the bony labyrinth (L). The planned trajectory (Tr) and the ideal trajectory as computed by the algorithm (broken-dotted line) are shown. **a** Planning situation from an inferior view; the angle δ describes the offset between the planned trajectory and the ideal trajectory with respect to the basal turn of the cochlea for a given cochleostomy target. Note that the ideal trajectory is running through the facial nerve. **b** The same plan as seen from an anterior view; the offset between the planned and the computed ideal trajectory in the basal turn plane is described by the angle ε.

Electrode Array Insertion

Electrode array insertion was performed by 2 experienced otolaryngologists using the same protocol. Ten free-fitting electrode arrays (MedEl Flex[28], 28 mm array length) were used for the experiments. The DCA tunnel was cleaned using irrigation and aspiration via the EAC. Hyaluronic acid was injected into a custom insertion tool (which provides alignment to the cochleostomy) for lubrication. Next, the electrode arrays were carefully straightened and slowly introduced into the tool lumen and the progression into the cochlea was observed with a 4 mm 30 degree endoscope through the EAC. Advancement of the electrode array was stopped at the point of first resistance. After completion of the insertion, the electrode arrays were fixed using sutures to prohibit movement during subsequent handling phases. During the experiments, the insertion time and tactile feedback of the insertion were recorded.

Postoperative Imaging and Data Analysis

Postoperative scans were acquired using the same protocol as in the preoperative phase with and without the implanted electrode arrays. The pre/postoperative datasets were registered by aligning the surfaces of the implanted fiducial screws (Amira 5). The accuracy of the drilled DCA tunnel was assessed by comparing the segmented tunnel position with the planned trajectory as previously reported [118]. The drilled trajectory target error, alignment (angles δ and ε), the actual cochleostomy position (θ_C), the implanted scala, the angular insertion depth, and the number of intracochlear contacts were assessed. Furthermore, 3D visualizations were generated for additional evaluation.

2.4 Results

Cochleostomy/Trajectory Computation and Planning

The preoperative imaging resolution and quality were sufficient for the identification of the specified landmarks and for the segmentation of the bony labyrinth. The presented script generated cochleostomy targets at positions inferior to the RW membrane. Visual inspection of the image data showed effective alignment of the computed trajectories with the basal turn. Preprocessing, including landmark identification, bony labyrinth segmentation, and computation of cochleostomy targets and trajectories, took approximately 15 min on average for each case. In all cases, the output of the script was used for subsequent trajectory planning. Due to a narrow facial recess, it was planned to sacrifice the chorda tympani in 3 cases (see Table 2.1).

Table 2.1. Summary of cochleostomy target and drill trajectory planning details.

	1R	1L	2R	2L	3R	3L	4R	4L	5R	5L
Distance to critical structures										
Facial nerve, mm	0.37	0.44	0.32	0.37	0.43	0.37	0.38	0.38	0.36	0.39
Chorda tympani, mm	0.00	0.12	0.00	0.00	0.53	0.22	1.18	1.17	0.33	0.37
EAC posterior wall, mm	0.90	0.55	0.45	0.45	1.85	1.60	2.34	1.89	0.62	0.90
Incus/Malleus, mm	2.36	2.60	3.02	2.64	2.95	2.78	3.11	2.55	2.88	3.01
Stapes, mm	0.62	0.65	0.68	0.77	0.65	0.80	0.69	0.74	0.58	0.51
Trajectory alignment										
Sacrificed chorda tympani	yes	no	yes	yes	no	no	no	no	no	no
Out of plane angle δ, °	12	8	7	11	15	12	12	11	14	10
In-plane angle ε, °	0	0	0	0	1	0	0	1	1	7
Cochleostomy position θ_C, °	10	12	12	12	4	8	12	12	4	4

1R/L to 5R/L are specimen identification numbers. See Fig. 2.4 for the alignment angles δ and ε, and Fig. 2.2 for the cochleostomy position angle θ_C.

DCA Drilling and Cochleostomy

Robotic DCA tunnel and cochleostomy drilling were feasible in every case (Fig. 2.5e). The accuracy at the cochleostomy target was measured at 0.30 ± 0.23 mm with a range of 0.05 to 0.79 mm. Four cases had broken screws which likely caused some degree of error in the registration process. In 2 of these cases a target error bigger than 0.35 mm occurred (Table 2.2). The target error was orientated anteriorly and posteriorly in specimens 1L and 1R, respectively. This caused penetration of the EAC posterior bony wall in specimen 1L and a close passage of the facial nerve in specimen 1R. As expected, the chorda tympani was damaged in specimens 2L and 2R.

Table 2.2. DCA target accuracy and insertion results.

	1R	1L	2R	2L	3R	3L	4R	4L	5R	5L
Broken registration screws	yes	yes	no	no	yes	no	no	no	no	yes
Target accuracy, mm	0.60	0.79	0.15	0.07	0.33	0.05	0.24	0.28	0.22	0.27
Insertion time, min	5	5	2	5	2	5	7	5	4	5
Intracochlear contacts	10	8	8	7	11	12	9	8	12	11
Angular insertion depth, °	330	270	300	210	360	420	360	290	350	300
Implanted scala	ST	SV	ST	ST	ST	ST	ST	ST	ST	ST

1R/L to 5R/L are specimen identification numbers.

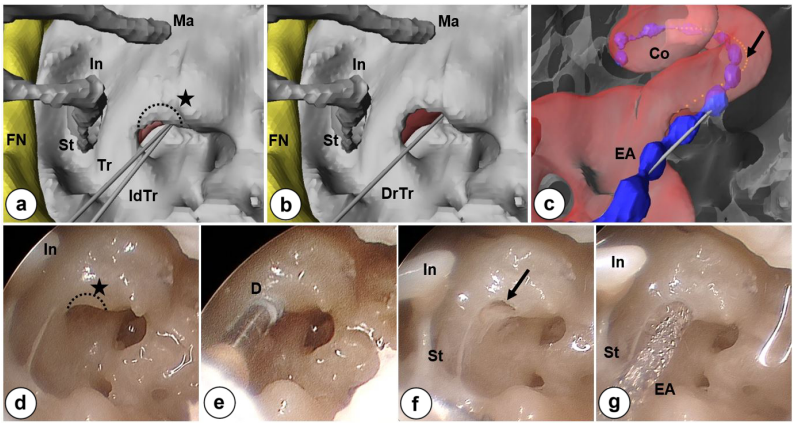

Fig. 2.5. 3D virtual view of the promontory and corresponding endoscopic photo documentation during cochleostomy drilling and array insertion in specimen 2R. The facial nerve (FN), the stapes (St), the long process of the incus (In), and the malleus (Ma) provide orientation landmarks. **a** The planned trajectory (Tr) and the computed ideal trajectory (IdTr) are shown. The cochleostomy (dotted semicircle) is aimed at drilling through the RW bony overhang (black star). **b** View of the promontory after cochleostomy and the corresponding drilled trajectory (DrTr). **c** Transparent view of the promontory after the insertion of the electrode array (EA). The cochlea (Co) and the centroid line as computed by the algorithm (arrow) are shown. **d** The promontory prior to cochleostomy drilling (dotted semicircle) at the RW bony overhang (black star). **e** Cochleostomy drilling with a 1 mm diamond burr (D). **f** The promontory with cochleostomy (arrow). **g** After insertion of the electrode array (EA).

Electrode Array Insertion

Endoscopic examination demonstrated correct alignment of the drilled DCA tunnel and insertion tool with the cochleostomy (Fig. 2.5f). Manual electrode array insertion was feasible in all cases (Fig. 2.5g). Full insertion as indicated by the mark on the electrode array was achieved in 2 of 10 cases with an average angular insertion depth of 319 degrees (Table 2.2). The total insertion procedure took 5 min on average. Postoperative radiological examination showed 9 of 10 cases of complete placement into ST and 1 case of SV insertion caused by a drilling target error of 0.79 mm (Fig. 2.6).

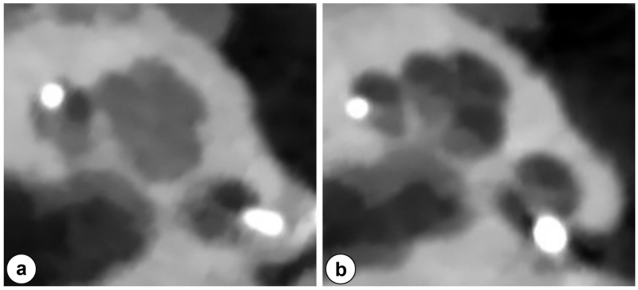

Fig. 2.6. Radiological evaluation of the insertion outcome in axial CBCT slices. **a** Left cochlea with SV insertion caused by a target drilling error of 0.79 mm orientated anteriorly (specimen 1L). **b** Complete ST insertion in a left cochlea (specimen 4L).

2.5 Discussion

This study investigates the applicability of a landmark based algorithm for patient-specific cochleostomy target and insertion trajectory computation. In the presented method, the lack of visualization of intracochlear structures in clinical computed tomography images is compensated for by the assumption that the basilar membrane position can be approximated based on specific landmark positions. These landmarks are easily identified and are based on a recognized scheme for cochlear visualization [87, 92, 96, 142, 145]. Furthermore, the landmarks enable the straight forward creation of a local cochlear coordinate system which has utility in the described planning method, as well as for other purposes (e.g., estimation of the cochlear size).

The algorithm computes cochleostomy targets starting from the RW and extending inferiorly along the promontory. The cochleostomy target positions match reports of previous histological and clinical studies [100]. Most of the chosen cochleostomy targets (θ_C) resulted in a RW related cochleostomy (Fig. 2.5).Using the presented approach, complete ST insertions were accomplished in 9 of 10 cases. In case 1L a SV insertion occurred due to an unusually large registration error, which caused an overall drilling error of 0.79 mm. Thus, although the planned trajectory intersected the ST, the drilled position deviated toward the SV.

In this study, as compared to previous tests with the robot system, a new self-drilling screw was implemented with the aim of a simpler and more straightforward procedure. The tips of these screws, however, were susceptible to breakage. The localization of the screws in the image data relies on an automatic fitting algorithm based on the shape of the screw. Thus, in cases where the tip of the screw is broken, the algorithm returns an incorrect position. The occurrence of broken screws was present in 4 samples, but a manual correction of the screw position was able to compensate for the bias in the automatic algorithm. Postoperative evaluation of the registration points revealed localization errors in the range of 0.20–0.50 mm in cases 1R and 1L. Thus, it is very probable that these broken screws were the cause of the high drilling error (0.60 and 0.79 mm) which had not occurred up till now in our collective experience with drilling approximately 30 specimens. Investigations are currently underway to find more robust self-drilling screws which are compatible with our workflow.

Postoperative radiographic assessment showed that the calculated ideal insertion trajectories were effectively aligned with the basal ST. Optimal insertion trajectories passed closely or intersected the facial nerve in all cases. This result closely corroborates those previously reported in a study using MicroCT data of human temporal bones [74]. Therefore, minimization of the angular deviation δ of the planned trajectory was mainly restricted by the position of the facial nerve. The average angular insertion depth in this study was observed to be significantly lower as in the previous experiments (319 degrees compared to 606 degrees) [144]. The main difference between the 2 studies is the fixation method (Sucquet versus Thiel), which is hypothesized to be the major factor that impeded higher insertion depths.

The segmentation of the bony labyrinth represents a crucial step in the presented algorithm. Therefore, errors introduced in this step may have an impact on the computation outcome. One outcome which may occur in case of over segmentation is that the cochleostomy drill would stop short of the endosteum. On the other hand, an under segmentation could possibly cause intracochlear trauma due to a zealous penetration of the cochlea. In this context, the application of additional information gained during the cochleostomy drilling (i.e., force and torque data) could be used to control the drilling depth to stop exactly at the endosteum. Moreover, it is clear that malformations in the basal region of the cochlea (e.g., basal turn ossification) have a strong impact on the computation routines used and are not compatible with the algorithm. Nevertheless, it is assumed that anatomical variations of the RW niche (e.g., an extremely narrow RW) do not influence the computation outcome as long as the RW landmark can be clearly identified [139].

2.6 Conclusions

This study shows that the landmark based approach is a valuable alternative for ST cochleostomy target and insertion trajectory planning in clinical imaging modalities. Although the script utilizes a manual landmark selection and a manual segmentation of the cochlea, targets can be planned in reasonable time (15 min). However, the automation of the manual segmentation process is the next step to significantly reduce time. Further, the presented cochleostomy approach is currently being evaluated using perimodiolar electrode arrays.

Acknowledgements

This work was financially supported by the Swiss National Science Foundation (NanoTera initiative project title Hear-Restore) and by the European Commission FP7 (project title HearEU). Cochlear electrode arrays were supplied by the Med-El Corporation, Innsbruck, Austria. The authors would like to thank Professor François Canovas, Professor Guillaume Captier, Franck Meyer, and Hubert Taillades, University of Montpellier, for the support during the experiments.

CHAPTER 3

MANUAL ARRAY INSERTION FOR MINIMALLY INVASIVE COCHLEAR IMPLANTATION

This chapter is published as:
Wimmer W, Bell B, Huth ME, Weisstanner C, Gerber N, Kompis M, Weber S, Caversaccio M. Cone beam and micro-computed tomography validation of manual array insertion for minimally invasive cochlear implantation. Audiol Neurotol 2014;19:22-30.

The concept of an insertion method applicable for a minimally invasive robotic approach is described. The procedure is tested in a cadaver model and evaluated by means of postoperative radiological imaging. The results suggest that the proposed insertion procedure is feasible and effective and can be applied for the minimally invasive implantation approach.

3.1 Abstract

Delivering CIs through a minimally invasive tunnel (1.8 mm in diameter) from the mastoid surface to the inner ear is referred to as DCA. Based on CBCT as well as MicroCT imaging, this in vitro study evaluates the feasibility and efficacy of manual cochlear electrode array insertions via DCA. Free-fitting electrode arrays were inserted in 8 temporal bone specimens with previously drilled DCA tunnels. The insertion depth angle, procedural time, tunnel alignment, as well as the inserted scala and intracochlear trauma were assessed. Seven of the 8 insertions were full insertions, with insertion depth angles higher than 520 degrees. Three cases of atraumatic ST insertion, 3 cases of probable basilar membrane rupture and 1 case of dislocation into the SV were observed (1 specimen was damaged during extraction). Manual electrode array insertion following a DCA procedure seems to be feasible and safe and is a further step toward clinical application of image-guided otological microsurgery.

3.2 Introduction

Since the inception of CIs, the facial recess approach has become the standard surgical technique to access the tympanic cavity and the cochlea. Currently, safe implant insertion through the facial recess generally requires a substantial mastoidectomy. Though the facial recess approach has remained largely unaltered, steps have been made toward reduced invasiveness (e.g. through the introduction of small incisions or microendoscopic procedures [77]). Furthermore, alternative surgical approaches utilizing the EAC to pass the CI electrode array into the tympanic cavity have been proposed. For example, the suprameatal, transcanal or pericanal approaches have drawbacks such as a steepened insertion angle, leading to a higher risk of electrode array kinking or damage to intracochlear structures [75]. Further, the risk of inflammation or infection of the EAC skin, and of consecutive electrode array extrusion, is increased.

Conversely, several methods of achieving a minimally invasive posterior tympanotomy or DCA have been proposed. These methods aim to avoid wide mastoidectomies while at the same time targeting the cochlea, for instance at the RW, at an optimal geometric angle relative to the basal turn. In this context, patient-specific stereotactic templates [146, 147] and skull-mounted [115, 116] or more conventional image-guided robotic approaches [113, 114] have been presented. Our group recently demonstrated that a DCA tunnel (1.8 mm in diameter) could be drilled with a targeting accuracy of 0.15 $\pm$ 0.08 mm using an image-guided robotic system [118]. As opposed to an electrode array insertion through a conventional mastoidectomy under direct visual feedback using standardized insertion tools, an insertion through small tunnel holes is more demanding due to restricted access for visual inspection and maneuvering of the electrode array. Thus, specific insertion tools, for both automatic and manual insertion, have been proposed [148, 149]. However, to our knowledge, no clinical data have been published on the effectiveness of such insertion tools.

Therefore, this study investigates the feasibility and efficacy of manually inserting a free-fitting CI electrode array through a minimally invasive DCA tunnel. We hypothesize that the electrode array can be threaded through the DCA tunnel and advanced into the cochlea utilizing common otological surgical instrumentation. The efficacy of the insertion is assessed by postoperative radiological eval-

uation of the implant position, the insertion depth angle and the alignment of the DCA trajectory using CBCT. Further, the extent of intracochlear trauma is evaluated by means of MicroCT imaging.

3.3 Materials and Methods

Surgical Preparation

As specimens, 4 Thiel-fixed human cadaver heads (n = 8 temporal bones) were used in this study [150]. Preceding the actual insertion experiment, 1.8 mm diameter DCA tunnels were drilled in each temporal bone of the specimens, using an image-guided robotic approach [118]. In short, titanium screws were placed in each temporal bone of the specimens to establish fiducial landmarks. Then, the specimens underwent CBCT imaging to permit trajectory planning [119] and high-accuracy patient-to-image registration [120]. Ultimately, the robotic system drilled a DCA tunnel from the surface of the mastoid bone through the facial recess to the center of the RW, as defined in the preoperative plan (Fig. 3.1).

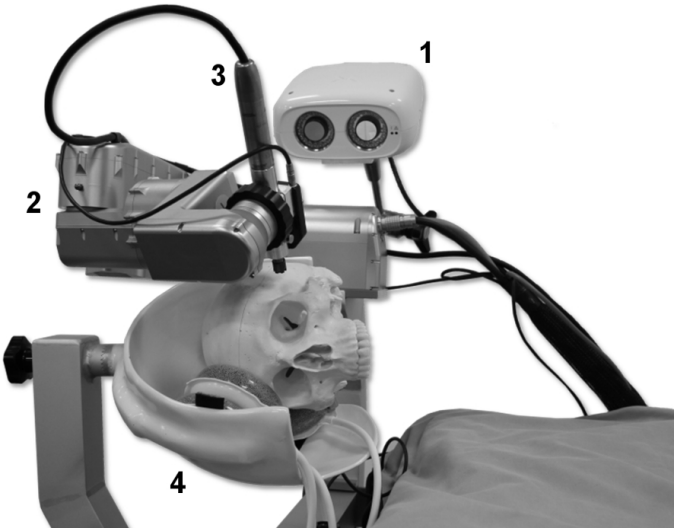

Fig. 3.1. Image-guided robotic system for DCA consisting of a high-accuracy optical tracking camera (1), robotic arm (2), surgical drill (3) and noninvasive head clamp (4).

The insertion study was carried out by first creating a conventional tympanomeatal flap through a retroauricular incision in order to provide access to and visibility of the cochlea promontory and the RW niche. Under microscopic view, the correct alignment of the DCA target relative to the RW was confirmed using an otological microneedle. The RW membrane was visualized by removing the bony overhang of the subiculum with a 1-mm otological Skeeter drill (Medtronic Xomed, USA). Bone dust was removed from the DCA tunnel and the promontory with saline irrigation and aspiration (1-mm suction tube). Additionally, a 1-mm-diameter sialendoscope (Karl Storz, Tuttlingen, Germany) was inserted into the DCA tunnel for further supervision (specimens 1R and 1L).

Electrode Array Insertion

Four standard electrode arrays (31.5 mm, 24 platinum contacts) and 4 Flex^{28} electrode arrays (28 mm, 19 platinum contacts) with free-fitting behavior were provided by the Med-El Corporation (Innsbruck, Austria). Electrode array insertion was performed manually, using CI temporal bone kit insertion instruments (Med-El Corporation) and an otological microneedle. The electrode arrays were inserted via the DCA tunnel through the RW into the ST. Advancement of the electrode array was stopped as soon as an insertion resistance was detected. Total insertion duration was defined as the time between the start of the retroauricular incision for the tympanomeatal flap and completion of the array insertion. The middle ear structures were inspected during preparation and after insertion. Finally, the proximal end of the electrode array was fixed in the EAC using packing material in order to avoid dislocation during temporal bone extraction.

Imaging

For CBCT and MicroCT imaging, the temporal bones including the implanted electrode arrays as well as 3 titanium fiducial screws were excised from the heads using an oscillating saw. The specimens were trimmed to fit into a 36-mm-diameter specimen holder for MicroCT imaging. Then, high resolution CBCT scans (ProMax 3D Max; Planmeca, Helsinki, Finland) were performed (voxel size: 150 µm isotropic; 90 kVp; 8 mA). The electrode array, the semicircular

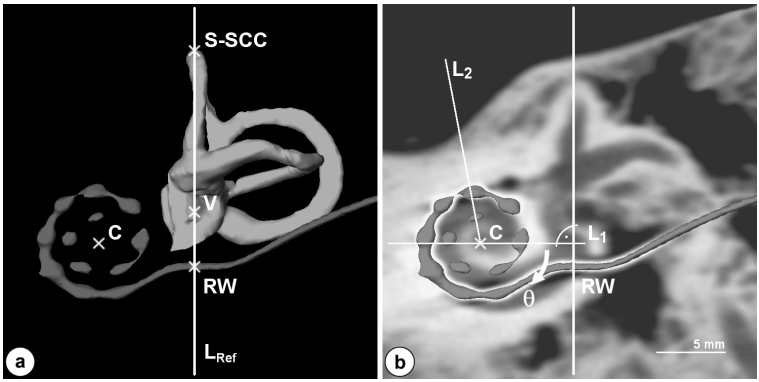

Fig. 3.2. Implanted electrode array, semicircular canals and vestibule segmented from CBCT data for insertion depth angle measurements. C = Center of electrode spiral. **a** The RW reference point is defined by the crossing of the implanted electrode array with an imaginary reference line (L_{Ref}) from the apex of the superior semicircular canal (S-SCC) through the center of the vestibule (V). **b** Same view, but superimposed onto a CBCT slice through the basal turn. The insertion depth angle (θ) is defined as the angle between L_1 and L_2, where L_1 is a line through the center of the electrode spiral (C) (perpendicular to L_{Ref}) and L_2 is the extrapolation of an imaginary line from C through the tip of the electrode array.

canals and the vestibule were segmented using Amira 5 visualization software (VSG, Burlington, Mass., USA). The insertion depth angle (θ) of each implanted array was measured as described in Xu et al. [151] (Fig. 3.2). Furthermore, the DCA tunnel orientation with respect to both the basal cochlear turn (angle δ) and the direction of the electrode array in the RW (angle ε) was assessed (Fig. 3.3). The CBCT scans were evaluated by an otolaryngologist and a neuroradiologist in order to determine the number of intracochlear contacts, the presence of array kinking and the intracochlear position of the electrode array with regard to the ST, scala media (SM) or SV in the basal, medial and apical turns of the cochlea. Complete placement of the electrode array with all contacts in the ST was considered a full insertion.

The samples were additionally scanned with a MicroCT device (μCT 40; SCANCO Medical AG, Brüttisellen, Switzerland) set at 70 kVp tube potential and 114 μA tube current. The dimensions of our samples limited the resolution of the scans to an isotropic voxel size of 18 μm. The electrode array was segmented and coregistered

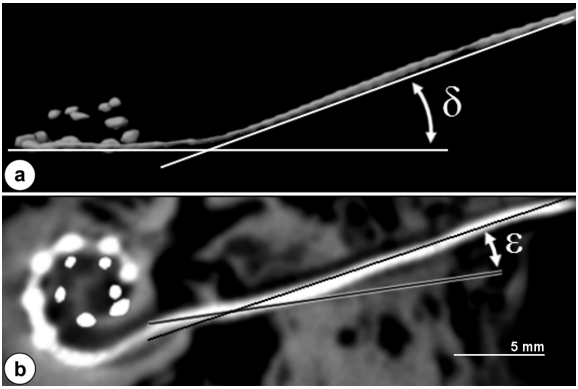

Fig. 3.3. DCA tunnel alignment described by the angles δ and ε, measured using CBCT scanning. **a** Axial view of the segmented electrode array implanted on the left side. The angle δ is measured between the axis of the DCA trajectory and the plane of the basal cochlear turn. **b** Coronal view of the cochlea and projected trajectory plane. The RW entry angle (ε) describes the deflection of the electrode array in the hook region of the basal turn and is measured between the axis of the DCA trajectory and the tangent of the electrode array in the center of the RW.

with the CBCT data using a surface alignment algorithm in Amira 5. After registration, the results found from the CBCT validation were compared and the intracochlear trauma was assessed by a neuroradiologist. For further visualization, MicroCT data was rendered as 3D volume model.

3.4 Results

Surgery/Electrode Array Insertion

The electrodes were manually inserted through the DCA tunnel into the cochlea via the RW. Manipulation and control of the insertion process was performed using common otological surgical instrumentation through the tympanomeatal flap. Insertion was achieved without explicit difficulties in all 8 temporal bones. After the tympanomeatal flap was elevated, the RW niche was completely visible in 6 of the 8 specimens. In 2 specimens (2R/2L; Table 3.1) about 1 mm of the EAC posterior wall was removed to adequately expose the RW niche (Fig. 3.4). Congruency between the end of the DCA trajectory and the center of the RW as a target of the preceding study was confirmed in all cases.

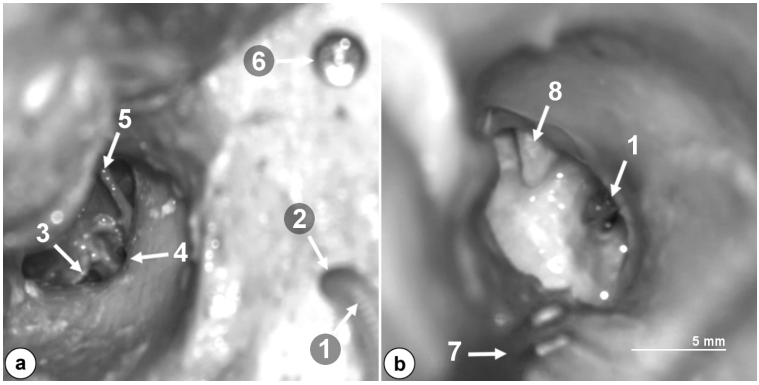

Fig. 3.4. Microscopic view of the tympanic cavity through the EAC during insertion in 2 different specimens. **a** The electrode array carrier (1) is manually advanced through the DCA tunnel (2) into the cochlea via the RW (3). To increase the visibility of the RW opening, approximately 1 mm of the EAC posterior wall was removed (4). The chorda tympani (5) and a fiducial screw (6) provide orientation marks. Specimen 2L. **b** The electrode array (1) is inserted into the RW and advanced when necessary using microforceps (7). The long process of the incus (8) provides an orientation landmark. Specimen 3L.

After insertion, no damage to the ossicles or the chorda tympani was observed. In 5 cases, the tip of the array had to be guided to the RW opening using a microforceps/-needle. Further advancement of the electrode array after introduction into the cochlea was possible

without using instrumentation in 4 specimens (Table 3.1). Seven of 8 insertions were full insertions, where further advancement was prevented by the silicone marker ring of the standard array or the increased diameter of the Flex^{28} array, respectively. In 1 case, 2 pairs of contacts were visible outside the cochlea when the first point of resistance was reached (specimen 3R; Fig. 3.5c). The average total duration for the insertion procedure was found to be about 35 min, excluding the time required for DCA drilling. An improvement of the absolute duration of the insertion procedure was observed over time (Table 3.1). A movie of the manual insertion process is provided as online supplementary video 1 (for all online suppl. material, see www.karger.com/doi/10.1159/000356165).

Imaging

The cochlea of specimen 1R was damaged during preparation, making only 7 temporal bones available for further evaluation. CBCT assessment demonstrated 3 cases of complete ST implantation (Fig. 3.6a). In the medial turn of specimens 1L, 2R and 3R, the electrode array was found to be in an intermediate position at the lateral wall without clear assignability to either the ST or SM (Fig. 3.5a). CBCT imaging showed smooth electrode array ascension and excluded any kinking. In the basal turn of specimen 4L, the basilar membrane was perforated and the array demonstrated a shift from the ST into the SV and back (Table 3.1; Fig. 3.7a). Three experiments conducted with the shorter Flex^{28} array (28 mm length vs. 31.5 mm in the standard array) led to an overinsertion by 30 to 80 degrees (specimens 2L, 4L and 4R; Table 3.1; Fig. 3.7c).

Evaluation of the MicroCT images confirmed the CBCT findings (Table 3.1). Again, the electrode array of specimens 1L, 2R and 3R could not be clearly assigned to either the ST or the SM due to an intermediate position at the lateral wall in the medial turn of the cochlea (Fig. 3.5b). The basilar membrane could be clearly identified in 6 of the 7 imaged cases; however, identification was not possible in specimen 2R. Electrode array displacement into the SV was confirmed for specimen 4L (Fig. 3.7b). MicroCT data permitted 3D rendering of the implanted specimens (Fig. 3.8). However, the 3D rendering to this point has provided no further insight into visualization of the basilar membrane (specimen 2R) or determination of the exact location of the intermediately positioned electrode arrays.

Table 3.1. Intraoperative in vitro study results and CBCT/MicroCT validation findings

	1R	1L	2R	2L	3R	3L	4R	4L
Specimen ID								
Age, years	80	80	51	51	97	97	77	77
Gender	female	female	female	female	female	female	male	male
Intraoperative observation								
Electrode array type	standard	standard	standard	Flex^{28}	standard	Flex^{28}	Flex^{28}	Flex^{28}
Drilling of EAC wall	no drilling	no drilling	posterior (1 mm)	posterior (1 mm)	no drilling	no drilling	no drilling	no drilling
Visual check of DCA tunnel/RW alignment	microneedle and endoscope	microneedle and endoscope	microneedle	microneedle	micro-needle	micro-needle	micro-needle	micro-needle
Introduction of array tip into RW	direct/no tool	direct/no tool	microneedle	microneedle	direct/ no tool	micro-forceps	micro-forceps	micro-needle
Advancement of electrode array	direct/no tool	direct/no tool	microclamp	microclamp	direct/ no tool	micro-forceps	micro-forceps	direct/ no tool
Total insertion duration, min	40	40	35	30	35	45	30	20
Intracochlear contacts	24 of 24	24 of 24	24 of 24	19 of 19	20 of 24	19 of 19	19 of 19	19 of 19
Postoperative CBCT validation								
Insertion depth angle θ, °	N/A	525	600	620	540	700	540	720
Scala implanted								
Basal turn	N/A	ST	ST	ST	ST	ST	ST	ST/SV
Medial turn	N/A	ST[a]	ST[a]	ST	ST[a]	ST	ST	SV/ST
Apical turn	N/A	-	-	-	-	-	-	ST
Array ascension	N/A	smooth	smooth	smooth	smooth	smooth	smooth	scala shift
DCA tunnel alignment angle δ, °	N/A	21	14	12	15	18	21	20
RW entry angle ε, °	N/A	15	10	25	5	4	18	10
Postoperative MicroCT validation								
Scala implanted								
Basal turn	N/A	ST	ST	ST	ST	ST	ST	ST/SV
Medial turn	N/A	ST/SM[a]	ST/SM[a]	ST	ST/SM[a]	ST	ST	SV/ST
Apical turn	N/A	-	-	-	-	-	-	ST
Intracochlear trauma[b]								
Basal turn	N/A	G0	G0	G0	G0	G0	G0	G3
Medial turn	N/A	G1/G2[a]	G1/G2[a]	G0	G1/G2[a]	G0	G0	G3
Apical turn	N/A	-	-	-	-	-	-	G0

1R/L to 4R/L are specimen identification numbers. - = no electrode array present; G0 = no trauma; G1 = basilar membrane displacement; G2 = basilar membrane rupture; G3 = dislocation into SV; N/A = not available.
[a]Not determinable; intermediate position between ST and SM. [b]Grading scale [152].

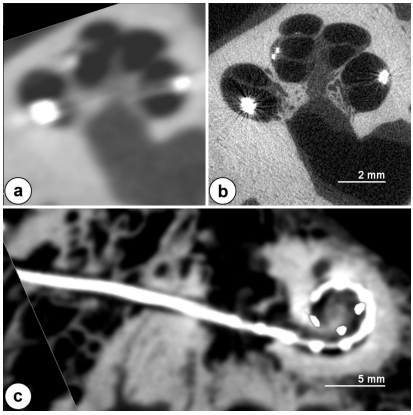

Fig. 3.5. Postoperative scans of the right cochlea with a partially inserted standard array in an intermediate position between the ST and SM (specimen 3R). Two pairs of electrode contacts are visible outside the cochlea. **a** Transversal CBCT image. **b** Corresponding MicroCT scan. **c** Coronal CBCT slice of the cochlear basal turn and projected DCA trajectory plane. Electrode array contacts present in the medial turn of the cochlea are overlaid.

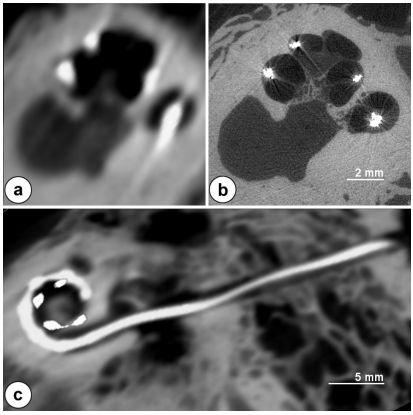

Fig. 3.6. Postoperative scans of the left cochlea, demonstrating atraumatic ST insertion of a Flex^{28} array (specimen 3L). **a** Transversal CBCT image. **b** Corresponding MicroCT scan. **c** Coronal CBCT slice of the cochlear basal turn and projected DCA trajectory plane. Electrode array contacts present in the medial turn of the cochlea are overlaid.

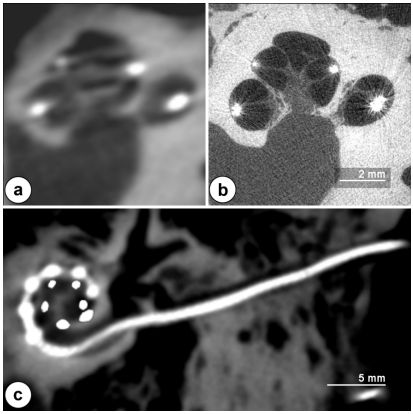

Fig. 3.7. Postoperative scans of the left cochlea with overinserted Flex^{28} array and basilar membrane rupture caused by dislocation of the array into the SV in the medial cochlear turn (specimen 4L). **a** Transversal CBCT image. **b** Corresponding MicroCT scan. **c** Coronal CBCT slice of the cochlear basal turn and projected DCA trajectory plane. Electrode array contacts present in the medial turn of the cochlea are overlaid.

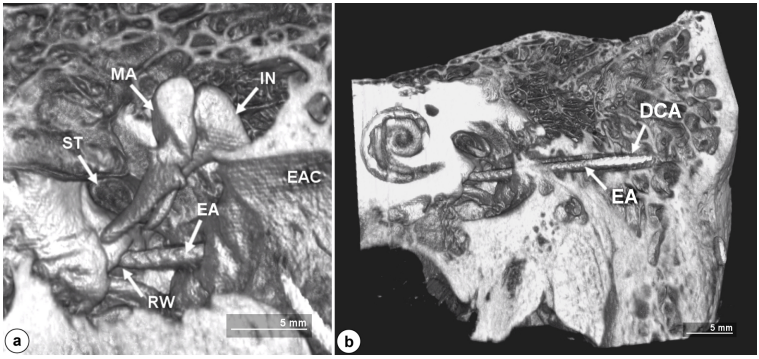

Fig. 3.8. 3D MicroCT data rendering of specimen 2L. **a** Magnified view of the tympanic cavity and the proximal portion of the EAC, showing the malleus (MA), incus (IN) and stapes (ST), as well as the electrode array (EA) entering through the RW. **b** Coronal view of the same specimen, demonstrating the course of the implanted EA through the DCA tunnel and the RW into the cochlea. An animated version of the 3D model is provided as online supplementary video 2.

3.5 Discussion

This study investigated the feasibility and efficacy of inserting a free-fitting CI electrode array through a minimally invasive DCA tunnel. The hypothesis that a complete array insertion through the DCA tunnel can be successfully performed utilizing common otological instrumentation was confirmed. The implanted electrode array position and DCA tunnel alignment were evaluated on postoperative CBCT images, and corresponding MicroCT data permitted assessment of intracochlear insertion trauma.

To our knowledge this is the first report of a CI insertion study conducted on Thiel embalmed specimens. This conservation technique is considered to realistically reproduce the color, mobility and flexibility of tissues in intraoperative situations and to offer excellent conditions for the training of surgical procedures in otology [153]. Negative aspects of the Thiel fixation are bad conservation of organs like the brain or bone marrow and the gelatinous texture of certain soft tissues (e.g. cartilage) [154]. Generally, MicroCT assessment showed good preservation of intracochlear structures. In 1 case the basilar membrane was not visible (specimen 2R). However, because the course of the electrode array implies the presence of a basilar membrane, we assume that this was caused by imaging artifacts. Further, we experienced little resistance during insertion, which may be related to the fixation method and explain the deep insertions achieved in this study. Therefore, we suggest further histological analysis to verify the applicability of the Thiel fixation method.

A tympanomeatal flap (routine for tympanic cavity access) as performed in this study is an additional step not common to the normal facial recess approach. Thus, the application of a tympanomeatal flap increases the risk of tympanic membrane perforation, subsequent electrode array exposure and middle/inner ear infections as compared with the standard approach. In this work, the tympanomeatal flap approach provided sufficient visual exposure to perform microscopic procedures such as cochleostomy drilling and sealing. The creation of the tympanomeatal flap accounts for an additional time of 15 minutes when compared with conventional insertion. Additionally, the tympanomeatal flap could be elevated prior to and for supervision of the tunnel drilling. Microscopic inspection and probing with an otological microneedle allows for sufficient evaluation of the DCA tunnel target alignment with the RW niche. An alternative method might

be direct endoscopic inspection and evaluation of DCA tunnel target alignment. Due to the suboptimal resolution of the sialendoscope, microscopic inspection was preferred in this study.

Previous studies have reported on the clinical applicability of CBCT petrous bone imaging for postoperative assessment of CI array positions. CBCT imaging is favorable due to its submillimeter spatial resolution and fast acquisition time (<20 s). Furthermore, CBCT has a reduced radiation exposure compared with conventional multislice CT imaging [155, 156]. The imaging resolution is, however, insufficient for the assessment of intracochlear trauma, and the radiologically measured electrode array diameter is exaggerated due to imaging artifacts [157]. We observed that the CBCT scans provided sufficient image resolution and quality for the estimation of the implanted scala in all cases imaged (Table 3.1). However, in 3 cases the electrode array was observed to be in the region of the SM (specimens 1L, 2R and 3R, all standard arrays; Fig. 3.5a). This intermediate position of the array, also described in Teymouri et al. [158], may refer to either a basilar membrane elevation with the array still being present in the ST or even a perforation with a shift into the SM. CBCT evaluation demonstrated that the DCA tunnel was not fully aligned with the basal turn of the cochlea in any specimen (angle δ; Table 3.1). While an optimized alignment may contribute to a reduction in insertion trauma, the results of this study do not suggest a correlation between trauma and the out-of-plane (δ) or in-plane (ε) components of the insertion angle. In many cases, the positions of structures of the facial recess, and a RW approach, will certainly limit an optimized insertion angle (minimization of δ and ε). Likewise, more optimal insertion angles could be achieved in some cases by abandoning the RW insertion in favor of a cochleostomy, which may lead to a reduction in insertion force, as proposed in Meshik et al. [74]. A strict RW insertion approach combined with the use of free-fitting electrode arrays resulted in bending at the RW entrance and the hook region of the basal turn of the cochlea, mainly in specimens 2R, 2L, 4R and 4L (Fig. 3.7c). Interestingly, this bending did not seem to cause additional trauma and the electrode insertion was perceived as smooth.

In this study, MicroCT scans were obtained to overcome aforementioned limitations of CBCT imaging and to assess intracochlear trauma. MicroCT may provide sufficient spatial resolution to display intracochlear membranous structures, but it is limited to in vitro ex-

aminations of small samples. Overall, the findings of the MicroCT evaluation matched the outcome of the CBCT investigation. Assessment of the MicroCT data confirmed 3 cases to be atraumatic ST insertions (specimens 2L, 3L and 4R, all Flex^{28} arrays; Fig. 3.6b). The image quality was not sufficient to resolve the difference between displacement and perforation and to estimate the exact intracochlear position of the electrode arrays in the intermediate position. Therefore, the intracochlear insertion trauma should be interpreted with caution and definitive evidence of atraumatic insertion cannot be obtained without further histological analysis of specimens 1L, 2R and 3R. The extent of intracochlear trauma was similar when compared with the results of previous temporal bone insertion studies with free-fitting electrode arrays (array length $\geq$ 25 mm) [45, 101, 138]. These studies report 25-27% of cases exhibiting basilar membrane/spiral ligament displacement or perforation, 0-9% of cases with dislocation of the array into the SV and 5-33% of cases with modiolus/osseous spiral lamina fracture compared with 43, 14 and 0%, respectively, in this study. In this work, deep insertions were achieved with nearly all arrays inserted more than one and a half turns ($\theta \geq 540°$; Table 3.1). The mean insertion depth angle of 606 degrees by far exceeds the values estimated in the studies reviewed (325-461 degrees). Nevertheless, a similar percentage of atraumatic insertion cases (43% compared with 33-59% reported in the literature) was found. Considering a hypothetical functionality of intracochlear contacts in specimens 2R and 3R, the electrodes near the RW would most probably provide no contribution to cochlear stimulation (Fig. 3.6c).

In conclusion, manual electrode array insertion following a minimally invasive mastoidectomy with supervision through a tympanomeatal flap is feasible and effective. In regard to electrode array insertion and imaging quality, Thiel-fixed temporal bones appear to be an adequate model for cochlear electrode insertion studies. The insertion depths achieved by this method were greater than those in the literature and should be considered when aiming for residual hearing preservation. Regarding trauma assessment, the approach presented cannot be truly compared with the current gold standard (conventional facial recess approach), although this may be achievable with further research into patient-specific insertion angle optimization. However, exclusively free-fitting electrode arrays were investigated in this study in a RW approach, and similar insertion investigations will be required in order to evaluate the nuances of

cochleostomy access and perimodiolar arrays with associated insertion tools.

The implantation technique presented must be considered within the context of the associated clinical workflow required for minimally invasive robotic CI surgery. Based on the results of a previous in vitro study [118] and currently undergoing investigations within the clinical environment, a total procedural time of about 2 hours is estimated for minimally invasive robotic cochlear implantation. Preoperative steps are fiducial screw implantation under local anesthesia (20 min), preoperative CBCT imaging (10 min) and subsequent trajectory planning (15 min). An intraoperative time of about 75 minutes is aimed for in the final state of the workflow, consisting of robotic system setup (15 min), patient preparation and registration (20 min), DCA drilling (5 min) and the implantation procedure presented in this study (35 min). The implant receiver can be fixed using any favored conventional technique including milling an implant bed and/or tie-down of the implant body. The electrode array can be inspected intraoperatively via the tympanomeatal flap, such as in case of acute implant failure. Likewise, management of cerebrospinal fluid gushers can be achieved through the tympanomeatal flap, for example using soft tissue packing (gelfoam, fat) and fibrin glue. It has yet to be seen to what extent postoperative scar formation occurs, but revisions may need to be performed under a conventional mastoidectomy and posterior tympanotomy.

In light of a future commercialization, the question of costs and benefits associated with the DCA procedure arises. Potential benefits like reduced invasiveness, shorter intraoperative time and possibility for outpatient treatment must be weighed against the substantial costs of such a system, which would greatly vary in different countries and cannot be specified within the scope of this work.

Acknowledgements

This study was financially supported in part by the Swiss National Center of Competence in Research, Computer-Aided and Image-Guided Medical Interventions (NCCR Co-Me) and the Nano-Tera.ch initiative, and the European Union's Seventh Framework Programme under HEAR-EU grant agreement No. 304857. Additional in-kind support was provided by Med-El Corporation (Innsbruck, Austria). The authors would like to thank Nane Boemke and Dr. Mathias

Bergmann, Institute of Anatomy, University of Bern, for the preparation of the cadaver specimens; Mark Siegrist, Department Clinical Research, University of Bern, for technical support in MicroCT scanning; and the Department of Neuroradiology, Inselspital Bern, for conducting CBCT imaging studies.

CHAPTER 4

SPEECH INTELLIGIBILITY IN NOISE WITH A SINGLE-UNIT COCHLEAR IMPLANT PROCESSOR

This chapter is published as:
Wimmer W, Caversaccio M, Kompis M. Speech intelligibility in noise with a single-unit cochlear implant audio processor. Otol Neurotol 2015; 36:1197-1202.

A novel CI audio processor that combines all parts in a single housing is examined. The new design causes a shift of the microphone position on the head of the CI recipient. A physical and computational model are used to investigate the influence of the microphone shift on speech intelligibility in noise. Further, the single-unit audio processor is evaluated in a clinical study. Both the models and the study indicate detrimental effects for speech in noise performance caused by the microphone shift.

4.1 Abstract

The Rondo is a single-unit CI audio processor comprising the identical components as its behind-the-ear predecessor, the Opus 2. An interchange of the Opus 2 with the Rondo leads to a shift of the microphone position toward the back of the head. This study aimed to investigate the influence of the Rondo wearing position on speech intelligibility in noise. Speech intelligibility in noise was measured in 4 spatial configurations with 12 experienced CIusers using the German adaptive Oldenburg sentence test. A physical model and a numerical model were used to enable a comparison of the observations. No statistically significant differences of the speech intelligibility were found in the situations in which the signal came from the front and the noise came from the frontal, ipsilateral, or contralateral side. The signal-to-noise ratio (SNR) was significantly better with the Opus 2 in the case with the noise presented from the back (4.4 dB, $p < 0.001$). The differences in the SNR were significantly worse with the Rondo processors placed further behind the ear than closer to the ear.

4.2 Introduction

Current behind-the-ear CI audio processors typically consist of 2 separate parts, the control unit and the transmission coil, which is connected by a cable. Recently, an audio processor that combines all the components in a single unit was introduced (Rondo; Med-El Corporation, Innsbruck, Austria). The potential advantages of the compact design might be an increase in wearing comfort and a reduction of the parts to be maintained. The Rondo consists of the identical electronic components and omnidirectional microphone as its predecessor, the Opus 2 (Med-El Corporation). Both audio processors are compatible with the identical implants and could be interchanged while using the same fitting. The position of the microphone with respect to the ear is different for the 2 devices. Whereas the microphone is located above the pinna in the Opus 2, it is located directly above the implant receiver coil and further behind the ear when using the Rondo. Early studies investigating bone-anchored hearing aids that are placed at a similar retroauricular position as the Rondo suggest that a backward shift of the hearing aid leads to compromising effects for speech in noise performance, if the noise is presented from the rear and omnidirectional settings are selected [159, 160]. It could be remarkable and of clinical importance to measure the hearing performance with the Rondo with respect to its wearing position.

The main goal of this investigation was to assess the speech intelligibility differences between the Opus 2 and the Rondo for different directions of the noise incidence. A physical and a numerical model were used to enable a comparison of the experimental results and to help to differentiate between random variations and systematic effects.

4.3 Materials and Methods

Participants

Twelve experienced Opus 2 users (7 female and 5 male subjects) aged 25 to 73 years (average age, 52 years) participated in the study. Ten subjects had profound hearing loss in both ears (unaided air conduction pure-tone average, >90 dB hearing level (HL)). Two subjects had profound hearing loss in the left ear and severe hearing loss (unaided air conduction pure-tone average, >70 dB HL) in the right ear. Seven participants were tested with the audio processors worn on the left side, and 5 were tested with the audio processors worn on the right side. The average duration of CI usage was 8 years (range, 2-18 years). All the participants were native German speakers with an average word recognition score of 81% (range, 70%-90%) with their CI at 60 dB sound pressure level (SPL) in the Freiburg monosyllabic word test [161].

Measurement Setup and CI Processor Fitting

All the experiments were conducted in a 6.0 x 4.1 x 2.2 m^3 anechoic chamber with an average, approximately frequency independent, reverberation time of 0.17 seconds. The subjects sat inside an array of 12 speakers (Control 1 pro; JBL Professional, Northridge, CA, USA) located in the horizontal plane with a spacing of 30 degrees. The speakers were placed at a distance of 1 m from the center of the subject's head at a height of 1.2 m. The measurements were controlled using a self-developed software. An external soundcard (US-2000; Tascam, Montebello, CA, USA) and an audio switch box (Audiobox; Merz Medizintechnik, Reutlingen, Germany) were used to drive the speaker array. The measurement setup and test room comply with the ISO 8253 series.

The Opus 2 and Rondo audio processors were programmed with the same maps that were used by the subjects in their daily life. Before starting the experiments, the subject's favorite program was selected, and the sensitivity and volume level were set equally for both processors. The Rondo was placed on the head according to the manufacturer's recommendations with the microphone opening pointing upward.

Study Protocol

This study was designed and conducted in accordance with the Declaration of Helsinki. The study protocol was approved by the local ethical committee in Bern (KEK-BE No. 084/13). All the subjects participated in a single session of approximately 2 hours. The speech in noise tests were performed once with the Opus 2 and once with the Rondo audio processor. No additional hearing aids and no earplugs were used. The speech intelligibility in noise was assessed using the German adaptive Oldenburg sentence test [162]. The test set consists of 40 test lists with 30 sentences and a speech babble noise with the same frequency spectrum as the long-term spectrum of the sentences. The noise was presented at a fixed level of 65 dB SPL, and the sentence signal level was adapted to estimate 50% word understanding, as proposed by the authors of the test. Four different spatial settings were used, as depicted schematically in Figure 4.1. The test sentences were always presented from the front, and the noise was presented from the front (S_0N_0), from the side ipsilateral to the CI (S_0N_{IL}), from the side contralateral to the CI (S_0N_{CL}), or from the back (S_0N_{180}). For each subject, 2 training lists were used before the experiments, and their results were discarded. The subjects were instructed to look straight ahead during the tests. The order of the tested CI audio processors, spatial configurations, and test lists were varied systematically to minimize the influence of training and fatigue effects.

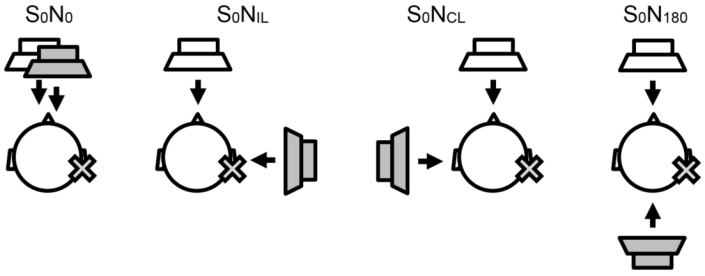

Fig. 4.1. Schematic representation of the 4 spatial configurations used for the speech in noise experiments. The settings were named according to the position of the CI audio processor (gray cross). S = signal (white speaker); N = noise (gray speaker); IL = ipsilateral; CL = contralateral.

Audio Processor Position

The azimuthal position of the Rondo was measured with a laser pointer. The Rondo was removed, and the laser pointer was magnetically attached above the implant receiver coil of the participants. A measuring arc with a centimeter scale was mounted above the speaker array. The subjects were asked to look straight ahead while the laser beam direction was measured. Figure 4.2 illustrates the measurement setup and the definition of the resulting azimuthal position θ.

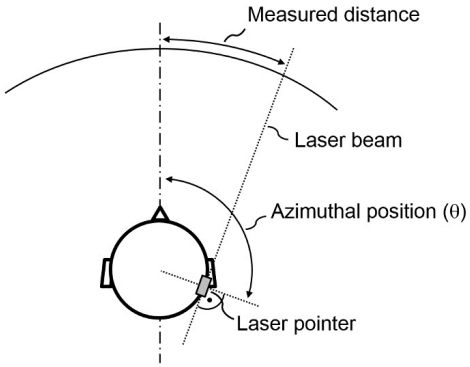

Fig. 4.2. The measurement setup for the determination of the azimuthal CI audio processor position. A laser pointer was magnetically attached above the implanted receiver coil of the participant. The azimuthal position θ could be calculated using the distance between the center of the head and the measuring arc (i.e., 1 m).

Modeling Speech Intelligibility in Noise

Because the speech understanding in noise was expected to vary between the subjects, the results were compared with 2 models to enable better separation of the random and systematic variations caused by the position of the microphone and the noise source. First, a head and torso simulator (Type 4128; Brüel & Kjær, Närum, Denmark), placed at the center of the test setup described previously was used as a physical model (Model 1). The measurements were performed with the Opus 2 positioned at $\theta_{OP} = 95°$ and the Rondo positioned between 90 and 180 degrees, in steps of 15 degrees (Fig. 4.3). As

the stimulus, Oldenburg speech babble noise was presented at 70 dB SPL from the same speakers used with the subjects (i.e., front, right, left, and rear). The microphone output signals were recorded using a microphone test device (Med-El Corporation) and an audio analyzer (R&S UPV; Rohde & Schwarz, Germany). A 16k FFT (Hamming-windowed, 100 averages) and a sampling rate of 48 kHz were used. The recorded power spectral densities were filtered with a moving average filter (M = 50). For each speaker and processor position, the spectral energy was calculated at the critical band central frequencies. Analogous to the speech in noise tests with the subjects, the improvement in the SNR was calculated as the difference between the SNR measured with the Opus 2 and Rondo. A speech intelligibility-weighted measure was used to correctly assign the contributions of different frequency bands to speech understanding [163]. The SNRs were calculated and weighted over 21 critical bands with center frequencies ranging from 150 to 8500 Hz [164].

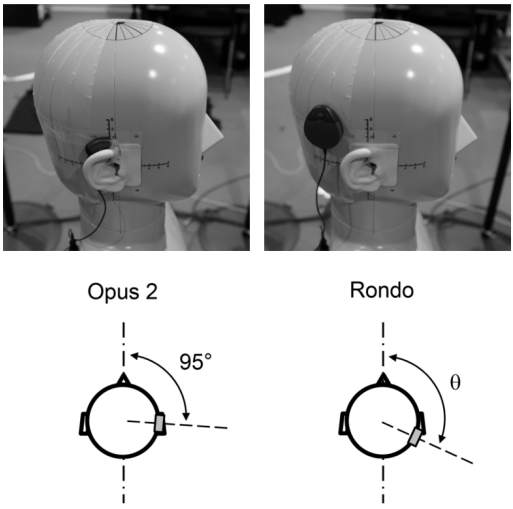

Fig. 4.3. Illustration of the experimental setup using a head and torso simulator. The Opus 2 microphone was positioned at 95 degrees, whereas the azimuthal position of the Rondo was altered ($90° \leq \theta \leq 180°$, $\Delta\theta = 15°$). For each configuration, the microphone output was recorded with stimuli from the front, ipsilateral, contralateral, or rear speaker.

Second, a numerical model (Model 2) was implemented to enable an evaluation of the influence of the azimuthal microphone position on speech intelligibility in noise. The approach of the plane harmonic wave diffraction around a rigid sphere was selected. Modeling the human head as a rigid sphere is a useful simplification for this study because it allows estimation of the influence of the microphone position without any effects of the pinna. Spherical models of the head have been shown to model the head shadow effect reasonably well [165]. The analytical formulas provided by Schwarz were used to compute the sound pressure phasor ratios on the sphere surface at different azimuthal positions for an incident sound wave [166]. As in previous studies, a head radius of 9.3 cm was assumed, and a speed of sound of 340 m/s was selected [165, 167]. In a manner that was similar to the experiment with the physical model, 2 separate sound sources were superposed according to the tested spatial settings to model the speech in noise experiments (Fig. 4.1). The improvement in SNR was calculated (Opus 2 vs. Rondo) and weighted with regard to the speech intelligibility, as described previously.

Data Analysis

The audiologic outcomes were assessed as improvement in the SNRs required for 50% word understanding with the Opus 2 and the Rondo. The 2-tailed Wilcoxon matched-pairs signed rank test was used to compare the experimental results. The data were analyzed using the Instat 3 software package (GraphPad, Inc., La Jolla, CA, USA).

4.4 Results

Speech in Noise Performance

The average improvement in the SNR for each tested spatial setting is illustrated in Figure 4.4. For the S_0N_0, S_0N_{IL}, and S_0N_{CL} configurations, the differences (average ± the standard deviation) in the speech understanding between the tested audio processors were small (-0.1 ± 1.6 dB, -0.8 ± 1.2 dB, and -0.6 ± 1.8 dB) and not statistically significant ($p = 0.90$, $p = 0.08$, and $p = 0.15$). In the S_0N_{180} configuration, the average SNR was significantly worse (-4.4 ± 1.7 dB, $p = 0.0005$) with the Rondo than with the Opus 2 processor. The results of the speech in noise tests are summarized in Table 4.1.

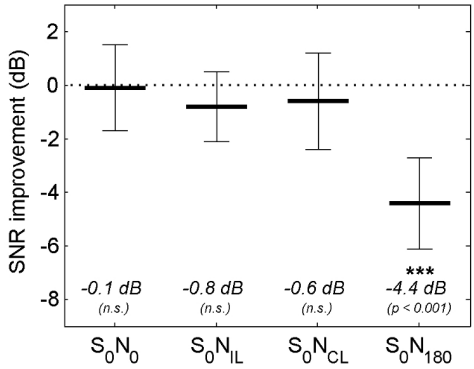

Fig. 4.4. The results of the speech in noise tests displayed as improvement in the SNR (Opus 2 vs. Rondo) required for 50% word understanding. The average SNR improvements (thick lines) and standard deviations are shown. The levels of statistical significance (***$p < 0.001$, n.s. = not significant) are displayed at the bottom of the figure for each configuration. The negative values denote better speech understanding with the Opus 2. See Figure 4.1 for a representation of the tested configurations.

Effect of the Microphone Position

Figure 4.5 shows the speech in noise test results as a function of the azimuthal position of the Rondo. The data are shown as the improvement (i.e., differences of the results with the Opus 2 minus the Rondo) in the SNR required for 50% speech understanding.

Table 4.1. The speech in noise results for the tested CI audio processors and spatial configurations.

Test configuration	SNR Opus 2, dB	SNR Rondo, dB	SNR improvement, dB (Opus 2 vs. Rondo)
S_0N_0	+0.6 (± 1.6)	+0.7 (± 2.1)	-0.1 (± 1.6)
S_0N_{IL}	+2.5 (± 2.5)	+3.3 (± 2.5)	-0.8 (± 1.2)
S_0N_{CL}	-1.7 (± 3.0)	-1.1 (± 2.7)	-0.6 (± 1.8)
S_0N_{180}	-0.9 (± 2.5)	+3.5 (± 3.3)	-4.4 (± 1.7)

The SNRs are listed as the average values (± the standard deviation).

The patient data, and the predictions of both models, are shown for each of the 4 spatial settings. The azimuthal position of the Rondo θ ranged from 93 to 135 degrees (average, 117 degrees). There was no statistically significant correlation between the Rondo position and the SNR improvement in the S_0N_0 (Pearson's correlation, r = -0.28, p = 0.38), S_0N_{IL} (r = 0.31, p = 0.33), and S_0N_{CL} (r = -0.11, p = 0.72) settings. A statistically significant correlation was found in the S_0N_{180} case (r = -0.65, p = 0.022), indicating that speech understanding becomes worse as the Rondo audio processor is situated further to the back.

Comparison to the Physical and the Numerical Model

The predictions of the physical and the numerical model are illustrated in Figure 4.5. Because the signal and the noise originate from the identical direction in the S_0N_0 setting, both models predict zero differences in the SNR. The asymmetric cases, S_0N_{IL} and S_0N_{CL}, reveal a systematic overestimation and underestimation, respectively, (approximately 1.5 dB) of the SNR improvement by the numerical model. This deviation is not observable in the symmetric S_0N_{180} case, in which the model predictions and physical measurements agree reasonably in the range of the observed Rondo positions (i.e., $90° \leq \theta \leq 135°$). The physical and the numerical model indicate a decline of the SNR improvement with increasing distance from the ear canal (approximately -1 dB per 10 degrees).

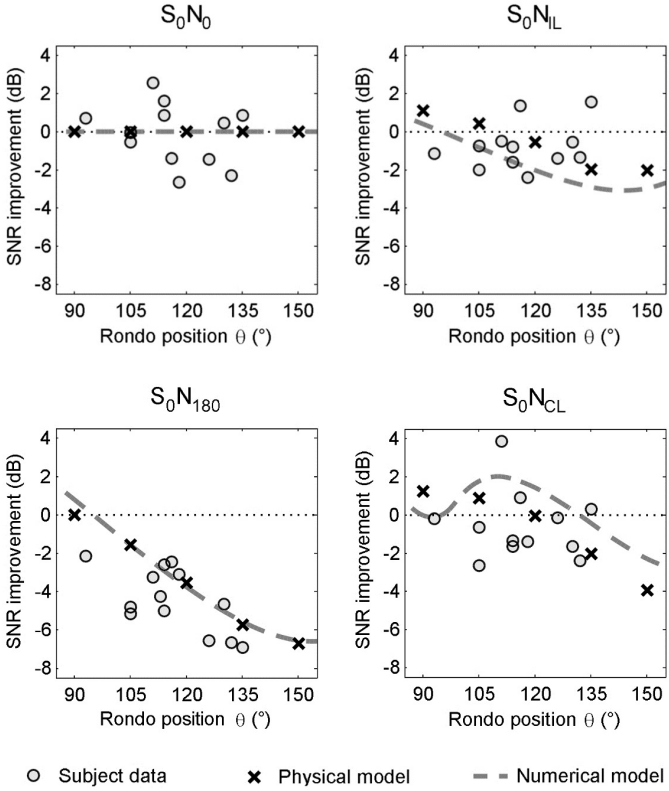

Fig. 4.5. SNR improvement as a function of the azimuthal Rondo position θ for the tested configurations. Each circle represents the difference of the speech in the noise test performances (i.e., Opus 2 minus Rondo) of 1 subject. The negative values denote better speech understanding with the Opus 2. The measurements of the physical model (Model 1) are represented by the black crosses. The predictions of the numerical rigid sphere model (Model 2) are plotted as dashed gray lines.

4.5 Discussion

This study investigated speech intelligibility in noise with the Opus 2 and the Rondo audio processors. There were no statistically significant differences between the devices in the S_0N_0, S_0N_{IL}, and S_0N_{CL} spatial configurations. This finding confirms that the audio processors are electronically identical and use the identical signal processing

technology. We found that CI users have poorer speech intelligibility with the Rondo in the case in which the masking noise is presented from the back (S_0N_{180}). Because of the omnidirectional characteristic of the microphone, the identical outcome might be measured in both devices when averaging the SNR over all the directions in the horizontal plane. Obviously, there are spatial settings in which the Rondo would provide better hearing in noisy conditions (e.g., when the speech is presented from the back and the noise is presented from the front). A recent study reported no compromising effects on speech reception in noise with the Rondo [168]. The study tested CI patients with single-sided deafness (SSD) in the S_0N_0 spatial configuration only. We believe that the spatial test configurations selected in our experiments offer a broader range of daily situations. More realistic situations could be provided with a multi-noise test setup, which was not used in this study. Assuming system linearity, a superposition of the 4 tested spatial settings might indicate the performance of the devices in a multi-noise situation (a worse performance with the Rondo is assumed).

In the S_0N_{180} situation, the subject data as well as the predictions of the physical and numerical model show that speech intelligibility decreases with increasing distances between the microphone and the ear canal. This finding indicates that CI users with the receiver/stimulator implanted in positions further behind the ear are expected to have higher difficulties in noisy situations when wearing a Rondo processor. Whereas this effect is visible, although partly obscured by the variations of the individual SNR improvements, both models clearly demonstrate the influence of the head shadow. It could be expected that the implementation of multi-microphone noise reduction systems might be beneficial in this context [169–172]. The influence of the microphone position on the sound localization performance of CI users might be of interest for further studies [173].

Overall, the tested subjects performed well in the speech in noise experiments. We observed similar speech reception thresholds (SRTs) (average $\pm$ the standard deviation, 0.6 ± 1.6 dB) in the S_0N_0 situation as in a previous study [174] with 28 unilateral CI users (0.7 ± 1.8 dB). The standard deviation of the test-retest differences is slightly higher than reported in another study (± 1.1 dB) [175]. We hypothesize that this finding is because of a worse than average speech perception (speech in quiet conditions) in our participants.

Acknowledgements

A Rondo audio processor was provided by the Med-El Corporation (Innsbruck, Austria) for the duration of the study. The authors thank Christoph Schmid and Thomas Wieland of the Department of Otolaryngology, Head and Neck Surgery, Inselspital Bern, for assistance in the CI audio processor fitting.

CHAPTER 5

SPEECH INTELLIGIBILITY IN NOISE WITH A PINNA EFFECT IMITATING COCHLEAR IMPLANT PROCESSOR

This chapter is published as:
Wimmer W, Weder S, Caversaccio M, Kompis M. Speech intelligibility in noise with a pinna effect imitating cochlear implant processor. Otol Neurotol 2016; 37:19-23.

The effect of a directional microphone system on speech intelligibility in noise is investigated. A new CI audio processor with a pinna compensation algorithm is evaluated in a clinical setting. The obtained results show improved speech reception thresholds with the directional microphone setting and indicate that CI recipients can profit from the pinna compensation algorithm.

5.1 Abstract

Objective: To evaluate the speech intelligibility in noise with a new CI processor that uses a pinna effect imitating directional microphone system.
Study Design: Prospective experimental study.
Setting: Tertiary referral center.
Patients: Ten experienced, unilateral CI recipients with bilateral severe-to-profound hearing loss.
Intervention: All participants performed speech in noise tests with the Opus 2 processor (omnidirectional microphone mode only) and the newer Sonnet processor (omnidirectional and directional microphone mode).
Main outcome measure: The SRT in noise was measured in 4 spatial settings. The test sentences were always presented from the front. The noise was arriving either from the front (S_0N_0), the ipsilateral side of the CI (S_0N_{IL}), the contralateral side of the CI (S_0N_{CL}), or the back (S_0N_{180}).
Results: The directional mode improved the SRTs by 3.6 dB ($p < 0.01$), 2.2 dB ($p < 0.01$), and 1.3 dB ($p < 0.05$) in the S_0N_{180}, S_0N_{IL}, and S_0N_{CL} situations, when compared to the Sonnet in the omnidirectional mode. There was no statistically significant difference in the S_0N_0 situation. No differences between the Opus 2 and the Sonnet in the omnidirectional mode were observed.
Conclusions: Speech intelligibility with the Sonnet system was statistically different to speech recognition with the Opus 2 system suggesting that CI users might profit from the pinna effect imitating directionality mode in noisy environments.

5.2 Introduction

CIs are a well-established and effective treatment for severe-to-profound sensorineural hearing loss. Although CI recipients are able to achieve high speech recognition scores in quiet surroundings, their performance in background noise is often impaired [128, 176–178]. The limited speech understanding in noise results from many factors such as the loss of fine spectral and temporal information and the narrow dynamic range available for electrical stimulation [36, 179]. To improve the speech in noise performance of CI users, several noise reduction strategies using single or multiple microphones have been implemented and evaluated in the past. Particularly directional microphones have consistently shown to ease the speech understanding in noisy environments. In commercial CI audio processors fixed and adaptive directional microphone systems can be differentiated. Fixed polar pattern systems provide benefits through spatial filtering of sound input from defined directions [36]. Previous studies have reported on SRT improvements of CI users around 3-7 dB, depending on the experimental conditions [36, 136, 170, 171, 179–182]. Even further improvements of the SRT can be achieved with adaptive systems which are capable of steering the zero-direction towards the noise source [35]. The speech in noise performance of CI recipients using adaptive systems was tested in several studies and showed SRT improvements between approximately 5 and 15 dB [169–172, 180, 181, 183, 184].

Recently, a new behind-the-ear processor with a dual microphone noise reduction system (Sonnet, Med-El Corporation, Innsbruck, Austria) was introduced. The CI audio processor comprises optional microphone directionality settings. The "natural" directionality mode combines a fixed directional pattern with a filter-implemented imitation of the natural pinna directivity. The primary aim of this study is to assess the benefit on speech intelligibility in noise with the Sonnet and the "natural" directionality mode in different spatial hearing situations. An evaluation of the efficacy of the directional microphone system is of clinical relevance and may give an idea of the expected benefit for CI users. Furthermore, the results are compared with the measurements with the older CI audio processor (Opus 2, Med-El Corporation).

5.3 Materials and Methods

Participants

Ten unilateral CI recipients with binaural severe-to-profound sensorineural hearing loss were included in the study. All the participants were native German speakers and experienced CI users. The details of the study participants are summarized in Table 5.1. The subjects were Opus 2 audio processor users and had never tried the Sonnet audio processor before this study.

Study Protocol

The study protocol was approved by the local Ethical Committee and was conducted according to the Declaration of Helsinki. The study was initiated, planned, and conducted at our institution and was not supported by any industrial partners. Three aided conditions were compared: the Opus 2 audio processor in the omnidirectional microphone mode (AP1), the Sonnet audio processor in the omnidirectional microphone mode (AP2-OMNI), and the Sonnet processor in the "natural" microphone mode (AP2-DIR). The "natural" mode introduces a fixed microphone directionality to imitate the natural pinna amplification of high frequencies arriving from the listener's front [8, 9, 185]. This setting was preferred over the optional, and potentially more effective, adaptive directional mode to exclude the influence of time-dependent filter coefficient readjustments and to avoid a situation-specific directionality. Before testing, the subjects indicated their most favored current program and setting on their

Table 5.1. Synopsis of the study participants.

Subject	Gender	Age years	CI Exp., years	Implant model	CI side	Active electrodes	Monosyllables at 60 dB, %	PTA of non-CI ear, dB HL
01	F	74	11	Combi40+	L	11	90	120
02	M	54	6	Pulsar	L	11	90	96
03	F	61	9	Pulsar	L	12	90	119
04	F	59	11	Combi40+	L	8	75	120
05	M	63	13	Combi40+	L	10	90	68
06	M	58	2	Concerto	L	12	80	103
07	F	27	6	Sonata	R	10	70	120
08	F	55	7	Sonata	L	12	70	106
09	M	69	18	Combi40	R	8	80	120
10	F	63	5	Sonata	R	8	75	113

Exp. = Experience; PTA = Pure tone average at 0.5/1/2/3 kHz.

own AP1. The AP1 fittings were converted to AP2-OMNI and AP2-DIR fittings according to the manufacturer's recommendation. The wind-noise reduction option was switched off and the sensitivity and volume levels of both audio processors were set to the same values for each participant. To assess the speech in noise performance, the German adaptive Oldenburg sentence test was used [162]. The test specific babble noise was presented at a fixed level of 65 dB SPL, and the sentence signal level was adapted to estimate the SRT at 50% word understanding. The subjects were tested in 4 different spatial situations: the speech signal was always presented from the front, whereas the noise was presented from the front (S_0N_0), from the side ipsilateral to the CI (S_0N_{IL}), from the side contralateral to the CI (S_0N_{CL}), or from the back (S_0N_{180}). At the beginning of the experiments, each subject went through 2 training lists, the results of which were not used for analysis. All the measurements were performed for the AP1, the AP2-OMNI, and the AP2-DIR mode. During the tests, the participants were instructed to keep their head in a straight position. No hearing aids or earplugs were used in the contralateral ear. To minimize training and fatigue effects, the order of the tested directionality modes, spatial situations, and test lists were varied systematically.

Test Room and Test Equipment

The speech in noise experiments were performed in an acoustic chamber (6.0 x 4.1 x 2.2 m^3) with a broadband reverberation time of 170 ms. The measurements were controlled using an in-house developed software. The speech and noise signals were amplified with an audio amplifier (Audiobox, Merz Medizintechnik, Reutlingen, Germany) and presented through Control 1 pro (JBL Professional, Northridge, CA, USA) loudspeakers positioned at a distance of 1.0 m from the listener.

Statistical Analysis

The experimental results were analyzed with a nonparametric repeated measures ANOVA (Friedman test, level of significance = 0.05). The two-tailed Wilcoxon signed rank test with Bonferroni correction was applied for paired posttests whenever a statistically significant effect was identified. The statistical analysis was performed using the Instat 3.10 software (GraphPad, Inc., La Jolla, CA, USA).

5.4 Results

Influence of the Pinna on Speech in Noise

At the time of the study it was not possible to record the microphone output signals of the new audio processor for an objective comparison between the microphone directionality patterns (AP2-OMNI, AP2-DIR). Therefore, 2 datasets (1 from published data and 1 from own measurements) were used to compare the influence of the pinna directivity in the tested speech in noise situations. The first dataset consisted of measurements performed in the above-mentioned test setup. A head and torso simulator (Brüel & Kjær, Type 4128, Nærum, Denmark) with built-in ear and pinna simulators (Brüel & Kjær, Type 4158/4159) was placed in the center of the loudspeaker array. The transfer functions of the ear simulators (case including pinna effects) and the microphone of an AP1 attached behind the ears (omnidirectional case) were measured from the directions according to the speech in noise tests. An audio analyzer (R&S UPV, Rohde & Schwarz, Germany) was used to generate sine sweep excitation signals and to record the microphone outputs. The second dataset was obtained from the head-related impulse response database provided by Kayser et al. [186]. The transfer functions were computed from the measurements of the "in-ear" and the "front" (omnidirectional, behind-the-ear microphone) situations (anechoic room, loudspeaker distance of 0.8 m). In both datasets the transfer functions were averaged over the left and the right side. For each test situation the signal-to-noise ratio was calculated over 21 critical bands and weighted according to their contribution to speech intelligibility [163]. The expected differences in SRT between the in-ear and behind-the-ear cases are shown in Table 5.2.

Speech in Noise Performance

Figure 1 shows the individual SRTs for the tested spatial situations and audio processors. A summary of the observed SRT improvements is listed in Table 5.3. The largest SRT difference between the AP2-OMNI and AP2-DIR modes was measured in the in the S_0N_{180} situation, showing an average improvement of 3.6 dB ($p < 0.01$). In the S_0N_{IL} and S_0N_{CL} situations, smaller but statistically significant SRT improvements were observed (2.2 dB, $p < 0.01$ and 1.3 dB, $p < 0.05$). As expected, the participants had comparable SRTs with

Table 5.2. The estimated SRT improvements caused by the directivity of the pinna simulator.

	Expected SRT improvement, dB	
Test situation	Acoustic chamber, D = 1.0 m, RT_{60} = 170 ms	Anechoic room [186], D = 0.8 m, RT_{60} < 50 ms
S_0N_0	0.0	0.0
S_0N_{IL}	1.3	0.3
S_0N_{CL}	1.4	1.9
S_0N_{180}	1.3	1.6

D = distance to the loudspeakers; RT_{60} = reverberation time.

Table 5.3. The SRT differences listed as the mean value, the standard deviation and the corresponding Bonferroni corrected probability.

	SRT difference, dB		
Test situation	AP1 vs. AP2-OMNI	AP1 vs. AP2-DIR	AP2-OMNI vs. AP2-DIR
S_0N_0	0.6 (±1.2), p = 0.39	0.6 (±1.4), p = 0.72	0.0 (±0.5), p = 1
S_0N_{IL}	0.1 (±1.1), p = 1	2.3 (±1.3), p = 0.006	2.2 (±0.8), p = 0.006
S_0N_{CL}	0.6 (±1.4), p = 0.70	1.9 (±1.6), p = 0.006	1.3 (±0.9), p = 0.012
S_0N_{180}	0.0 (±1.3), p = 1	3.7 (±1.8), p = 0.006	3.6 (±1.4), p = 0.006

AP1 = Audio processor 1; AP2-OMNI = Audio processor 2 (omnidirectional mode);
AP2-DIR = Audio processor 2 (fixed directional mode).

the AP2-OMNI and AP2-DIR modes in the S_0N_0 situation. There is no advantage of directional processing, because the signal and noise sources are not spatially separated. No statistically significant differences were measured between the 2 conditions with omnidirectional microphone modes (AP1 and AP2-OMNI). This shows that the participants had a similar speech in noise performance with both tested CI audio processors.

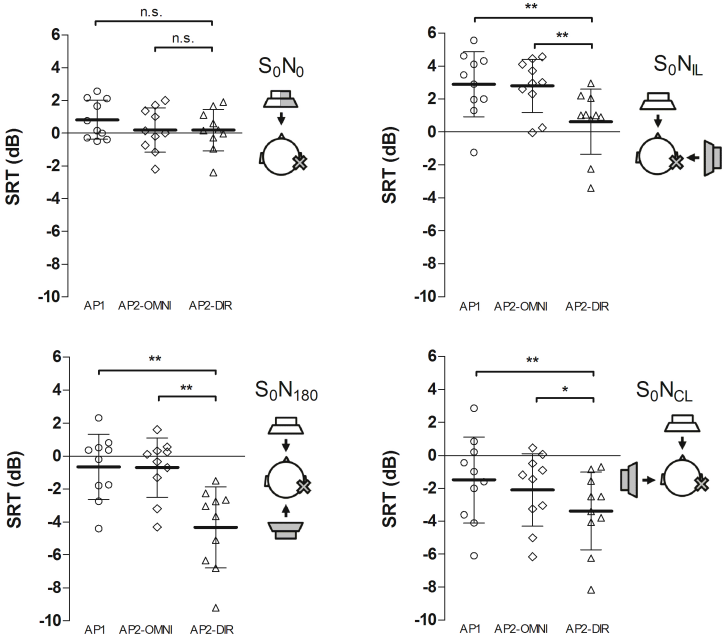

Fig. 5.1. The individual SRTs for the tested spatial situations and audio processors. Lower values denote better speech intelligibility in noise. The lines show the mean SRT and the standard deviation. The brackets show the level of statistical significance (n.s. = not significant, *p $<$ 0.05, **p $<$ 0.01). The position of the tested CI audio processor is indicated by a gray cross. S = Signal (white speaker), N = Noise (gray speaker), IL = Ipsilateral, CL = Contralateral, AP1 = Audio processor 1, AP2-OMNI = Audio processor 2 (omnidirectional mode), AP2-DIR = Audio processor 2 (fixed directional mode).

5.5 Discussion

This study assessed the influence of a pinna directivity imitating directional microphone mode on speech intelligibility in noise. The directional mode yielded equal or better SRTs when compared to the omnidirectional mode and caused no negative effects on the speech intelligibility in the tested situations. Therefore, patients using the new CI audio processor can be expected to benefit from the "natural" directional microphone setting in noisy environments.

Better SRTs were observed in all situations with spatially separated speech and noise signals using the "natural" directionality mode. An immediate improvement in SRT was found for all participants, regardless of the implant type and number of active stimulation channels. The largest SRT improvements were observed in the S_0N_{180} case, indicating that the masking noise from behind is effectively attenuated by the directional microphone system. The comparison of the SRTs between the S_0N_{IL} and the S_0N_{CL} cases shows an average head shadow effect in the range of 4-5 dB.

In the S_0N_0 situation, the participants performed well and achieved SRTs ranging from -2.4 to 2.6 dB. Comparable SRTs were measured with the AP1, AP2-OMNI, and AP2-DIR modes. As expected, no benefits for the speech reception are introduced by the directional microphone system, because both the test sentences and the noise were presented from the same speaker. In addition, the similar SRTs indicate that no disadvantageous effects on the speech intelligibility were introduced by the directional filtering algorithm.

There are several factors limiting a comparison of our results to the findings of previous studies, specifically the differences in the tested microphone directionality strategies, additionally applied noise suppression algorithms, differences in the test conditions (single-noise vs. multinoise), the measurement set-up (i.e. the distance, position and directionality of the loudspeakers), and the room characteristics (reverberation time). The SRT improvements found in this study lie within the range of previously reported findings using fixed directionality microphone systems [36, 136, 170, 171, 179–182].

The estimation model shows no SRT differences in the S_0N_0 situation, because the speech and noise originate from the same source (Table 5.2). In the S_0N_{180} and S_0N_{IL} situations, the SRT improvements as estimated from the datasets were smaller than observed with the tested CI users. A more comparable estimation was found in the

S_0N_{CL} situation. The validity of the estimation model is obviously limited, nevertheless, it indicates that SRT improvements because of the pinna effect can be expected in the experimental set-up. The differences between the estimated and measured SRT values suggest that the AP2-DIR mode provides a stronger directionality toward the front than a natural pinna. A hypercardiod polar pattern for frequencies above 2 kHz was reported to be sufficient for a compensation of the pinna effect in behind-the-ear hearing aids [185]. Currently there is, however, no data available for an objective evaluation of the directionality pattern provided by the AP2-DIR setting.

The speech in noise tests were performed with a single-noise source. Considering a multinoise scenario, the mean expected signal-to-noise ratio benefit could be estimated by a superposition of the tested situations because of the linearity of the microphone inputs in the fixed directionality mode. It is expected that a bigger benefit for speech intelligibility in noise can be achieved with the adaptive directionality mode of the CI processor. The evaluation of the adaptive directionality mode, however, lies beyond the scope of the presented work.

The identical test setup was used in a previous study investigating the speech in noise performance with a single-unit CI audio processor of the same manufacturer [187]. The study showed that an omnidirectional microphone placed further behind the ear leads to worse SRTs in the S_0N_{180} situation. A directional microphone system, such as the one investigated in this study, may compensate for the disadvantage caused by the shift of the microphone position.

The participants had similar SRTs in all tested situations with the AP1 and the AP2-OMNI conditions. This indicates that the interchange of the CI audio processors and the conversion/transfer of the fittings between the processors had no negative effects on the speech reception of the participants. The subjects tested in this study represent a cohort in which bilateral implantation should be preferred [55]. It is assumed that the pinna effect imitating directional microphone may provide benefits for patients with bilateral CIs. In the same way, the influence of the directional microphone system on sound localization may be interesting. This was not evaluated in the presented work and is subject to ongoing studies.

CHAPTER 6

CONCLUSIONS AND OUTLOOK

This chapter gives an overall conclusion about the work presented in the thesis. The contributions and limitations of the research projects are discussed and an outlook on upcoming work is described.

In this thesis, approaches from several disciplines were presented with the aim to improve the treatment efficacy of current CI systems. Computer-assisted methods and surgical procedures for minimally invasive cochlear implantation were developed and evaluated in cadaver models. Furthermore, novel CI audio processors and front-end signal processing technologies were examined about their impact on speech intelligibility in noise using computational models and audiological experiments.

6.1 Minimally Invasive Cochlear Implantation

The work presented in the first 2 chapters contributes to the workflow needed in the clinical application of the robotic DCA system designed at the University of Bern. A preoperative planning paradigm that accounts for insertion-related aspects was developed. The method was evaluated in a cadaver model and achieved 9 of 10 insertions into the ST. The case of the SV insertion is not ascribed to the planning method, because of the registration error caused by a broken fiducial screw. Our group continues on the advancement of the preoperative planning methods to further automate the proposed paradigm and to incorporate additional features that can be also valuable in conventional surgery, e.g., the preoperative selection of electrode arrays that fit the patient's residual hearing and anatomical situation. It has to be pointed out that the potential advantages of the proposed methods with regard to structural preservation are subject to clinical evaluations.

Furthermore, a clinically applicable CI electrode array insertion method was developed and tested. The procedure demonstrated both safe and effective insertions. It could be argued that the tympanomeatal flap may oppose the minimally invasive DCA concept. However, for safety reasons the tympanomeatal flap is intentionally kept in the clinical procedure during the first-in-man clinical study. It allows an immediate reaction in the case of unanticipated problems during the array insertion. In the meantime, our group has been working on a strategy that avoids the tympanomeatal flap. First, the procedure would involve a microendoscope inserted through a small incision in the tympanic membrane for supervision. Then, the robotic system can be used to not only drill the DCA but also to automatically perform the ST access. The feasibility of an atraumatic access through the combination of preoperative planning and force-sensing

data has already been demonstrated [188]. After the endosteum is exposed, the tympanic cavity can be cleaned with irrigation and suction administered through the DCA. Finally, an insertion guide tube could be inserted through the DCA tunnel to bypass the tympanic cavity and to facilitate an insertion controlled only from the mastoid surface. A first prototype of such an insertion tool is currently under investigation. The limitations of the suggested approach avoiding the tympanometal flap are the sealing method of the electrode array after insertion and the management of bleeding. The latter issue can be only evaluated in vivo. Possible solutions for sealing would be to introduce grafting material through the tympanostomy or to develop electrode arrays with dedicated sealing mechanisms. A further improvement envisioned is the application of the robotic manipulator for the insertion itself. The force-sensing components and the high accuracy could be valuable for an automatically controlled insertion procedure.

6.2 CI Audio Processor Front-End

The second part of the thesis evaluated novel audio processor designs and front-end signal processing with regard to speech intelligibility in noise. The results of both presented studies provide clinically relevant data about the expected outcome with the CI audio processors.

The study investigating the single-unit audio processor demonstrates the impact of the microphone position on speech in noise performance. A direct correlation between the position of the omnidirectional microphone on the head and the measured SRT was shown. A position shift to the back of a few centimeters caused a significantly reduced speech intelligibility in the experimental setup. This finding is important for the counselling of CI recipients prior to upgrading to the new processor. In addition, the results could be used to improve newer versions of the single-unit CI processor. The demonstrated effect might as well be considered in the placement of the microphone in future totally implantable CI systems.

A way to improve speech intelligibility in noise is the implementation of directional multimicrophone systems. In the second audiological study, the evaluation with the pinna effect imitating directional microphone showed an immediate benefit for the tested CI users. Thus, at least for adults, the directional microphone setting should be suggested as a standard for the fitting procedure with this model.

In the presented studies, the identical experimental configurations were used and the investigated audio processors were tested against the same preceding model. This enables a direct comparison between the CI audio processors of both studies. The single-unit processor certainly aims at different demands of CI users (e.g., optical appeal), however, the differences in the speech in noise performance compared with the directional microphone processor are striking. Therefore, from an audiological point of view, the CI audio processor with the directional microphone functionality should be preferred. A consideration of the results of both studies further suggest that the position-introduced drawback of the single-unit processor can be overcome by the implementation of directional microphone systems.

An even higher benefit for the speech intelligibility in noise can be expected from adaptive beamforming algorithms. The investigated pinna effect imitating audio processor additionally offers an adaptive microphone directionality setting. An evaluation of the performance of the adaptive beamformer is of clinical relevance, but requires the understanding of the dynamic parameters of the algorithm before testing with subjects.

As suggested in the studies, an implementation of more representative conditions for the speech in noise experiments should be undertaken. One way to achieve a more realistic test environment would be the application of test scenarios with diffuse background noise. For that reason, multi-noise tests are currently developed and evaluated for future speech intelligibility studies in our institution.

In this thesis, several aspects of cochlear implantation were addressed and multidisciplinary methods were applied to improve the efficacy of current CI systems. Nevertheless, open questions remain to be addressed to further advance the presented methods and concepts.

LIST OF TABLES

LIST OF FIGURES

REFERENCES

[1] WHO global estimates on prevalence of hearing loss (Internet, accessed 24 September 2015). Geneva: World Health Organization; 2012. Available from: www.who.int/pbd/deafness/estimates.

[2] Reiter R, Pickhard A, Brosch S. Hearing impairment and language development (in German). *Laryngorhinootologie* 2012; 91:550–559.

[3] Ciorba A, Bianchini C, Pelucchi S, Pastore A. The impact of hearing loss on the quality of life of elderly adults. *Clin Interv Aging* 2012; 7:159–163.

[4] Eshraghi A, Nazarian R, Telischi F, Rajguru S, Truy E, Gupta C. The cochlear implant: historical aspects and future prospects. *Anat Rec* 2012; 295:1967–1980.

[5] Shaw EA. The external ear. Handbook of Sensory Physiology (Vol. 1) Auditory System. Ed. by Keidel W, Neff W. New York: Springer Verlag, 1974:455–490.

[6] Mehrgardt S, Mellert V. Transformation characteristics of the external human ear. *J Acoust Soc Am* 1977; 61:1567–1576.

[7] Ballachanda BB. Theoretical and applied external ear acoustics. *J Am Acad Audiol* 1997; 8:411–420.

[8] Shaw EA. Transformation of sound pressure level from the free field to the eardrum in the horizontal plane. *J Acoust Soc Am* 1974; 56:1848–1861.

[9] Blauert J. Spatial Hearing. The psychophysics of human sound localization. Cambridge, MA: The MIT Press, 1997:108–111.

[10] Oldfield SR, Parker SPA. Acuity of sound localisation: A topography of auditory space. II. Pinna cues absent. *Perception* 1984; 13:601–617.

[11] Kompis M. Audiologie. 3rd Ed. Bern: Verlag Hans Huber, 2013.

[12] Plattig K. Äusseres Ohr und Mittelohr. Physiologie des Gehörs. Ed. by Keidel W. Stuttgart: Georg Thieme Verlag, 1975:50–62.

[13] Borg E, Counter S, Rösler G. Theories of Middle-Ear Muscle Function. The acoustic reflex: basic principles and clinical applications. Ed. by Silman S. Orlando, Florida: Academic Press, Inc., 1987:86–90.

[14] Mukerji S, Windsor AM, Lee DJ. Auditory brainstem circuits that mediate the middle ear muscle reflex. *Trends Amplif* 2010; 14:170–191.

[15] Hayes SH, Ding D, Salvi RJ, Allman BL. Anatomy and physiology of the external, middle and inner ear. Handbook of Clinical Neurophysiology. Vol. 10. 2013:3–23.

[16] Würfel W, Lanfermann H, Lenarz T, Majdani O. Cochlear length determination using Cone Beam Computed Tomography in a clinical setting. *Hear Res* 2014; 316:65–72.

[17] Rask-Andersen H, Liu W, Erixon E, et al. Human cochlea: Anatomical characteristics and their relevance for cochlear implantation. *Anat Rec* 2012; 295:1791–1811.

[18] Ulehlová L, Voldrich L, Janisch R. Correlative study of sensory cell density and cochlear length in humans. *Hear Res* 1987; 28:149–151.

[19] Hardy M. The length of the organ of Corti in man. *Am J Anat* 1938; 62:291–311.

[20] Lang J. Klinische Anatomie des Ohres. Wien: Springer-Verlag, 1992:164–166.

[21] Hesse G. Grundlagen der Anatomie und der Physiologie des Innenohres. Innenohrschwerhörigkeit. Ed. by Hesse G. Georg Thieme Verlag, 2015:14–15.

[22] Rinsdorf G. Ohrfunktionstheorien, Mathematik der Basilarmembran. Physiologie des Gehörs. Ed. by Keidel W. Stuttgart: Georg Thieme Verlag, 1975:64–72.

[23] Olson ES, Duifhuis H, Steele CR. Von Bekesy and cochlear mechanics. *Hear Res* 2012; 293:31–43.

[24] Sellick PM, Patuzzi R, Johnstone BM. Measurement of basilar membrane motion in the guinea pig using the Mössbauer technique. *J Acoust Soc Am* 1982; 72:131–141.

[25] Kandel E, Schwartz J, Jessell T, Siegelbaum S, Hudspeth A. Perception. Principles of Neural Science. New York: McGraw-Hill, 2000:654–681.

[26] Pfiffner F, Caversaccio M, Kompis M. Audiological Results with Baha in Conductive and Mixed Hearing Loss. Implantable Bone Conduction Hearing Aids. Ed. by Kompis M, Caversaccio M. Basel: Karger, 2011:73–83.

[27] Reinfeldt S, Håkansson B, Taghavi H, Eeg-Olofsson M. New developments in bone-conduction hearing implants: a review. *Med Devices* 2015; 8:79–93.

[28] Puria S. Middle Ear Hearing Devices. The Middle Ear: Science, Otosurgery, and Technology. Ed. by Puria S. New York: Springer, 2013:273–308.

[29] Zarandy MM, Rutka J. Diseases of the inner ear: A clinical, radiologic and pathologic atlas. 2010:1–93.

[30] Kompis M, Pfiffner F, Krebs M, Caversaccio MD. Factors influencing the decision for baha in unilateral deafness: The bern benefit in single-sided deafness questionnaire. Implantable Bone Conduction Hearing Aids. Ed. by Kompis M, Caversaccio M. Basel: Karger, 2011:103–111.

[31] Senn P, Kompis M, Caversaccio M. Hören: Cochleaimplantate. Interventionelle Neurophysiologie. Ed. by Classen J, Schnitzler A. Stuttgart: Georg Thieme Verlag, 2013:258–267.

[32] Djourno A, Eyriès C, Vallancien B. Premiers essais d'exitation électrique du nerf auditif chez l'homme par micro-appareils inclus à demeure. *Bull Acad Nat Med* 1957; 141:481–483.

[33] Mudry A, Mills M. The early history of the cochlear implant: a retrospective. *JAMA Otolaryngol Head Neck Surg* 2013; 139:446–553.

[34] Zeng F, Canlon B. Recognizing the journey and celebrating the achievement of cochlear implants. *Hear Res* 2015; 322:1–3.

[35] Kompis M, Bertram M, François J, Pelizzone M. A two-Microphone noise reduction system for cochlearimplant users with nearby microphones - part I: signal processing algorithm design and development. *Eurasip J Adv Sig Pr* 2008; DOI: 10.1155/2008/647502.

[36] Kokkinakis K, Azimi B, Hu Y, Friedland DR. Single and multiple microphone noise reduction strategies in cochlear implants. *Trends Amplif* 2012; 16:102–116.

[37] Wilson BS, Finley CC, Lawson DT, Wolford RD, Eddington DK, Rabinowitz WM. Better speech recognition with cochlear implants. *Nature* 1991; 352:236–238.

[38] Büchner A, Frohne-Büchner C, D. Battmer R, Lenarz T. Two years of experience using stimulation rates between 800 and 5000 pps with the clarion CII implant. *International Congress Series* 2004; 1273:48–51.

[39] Kiefer J, Hohl S, Stürzebecher E, Pfennigdorff T, Gstöttner W. Comparison of speech recognition with different speech coding strategies (SPEAK, CIS, and ACE) and their relationship to telemetric measures of compound action potentials in the nucleus CI 24M cochlear implant system. *Audiology* 2001; 40:32–42.

[40] Büchner A, Beynon A, Szyfter W, et al. Clinical evaluation of cochlear implant sound coding taking into account conjectural masking functions, MP3000™. *Cochlear Implants Int* 2011; 12:194–204.

[41] Donaldson GS, Dawson PK, Borden LZ. Within-subjects comparison of the HiRes and Fidelity120 speech processing strategies: speech perception and its relation to place-pitch sensitivity. *Ear Hear* 2011; 32:238–250.

[42] Hochmair I, Hochmair E, Nopp P, Waller M, Jolly C. Deep electrode insertion and sound coding in cochlear implants. *Hear Res* 2015; 322:14–23.

[43] Wouters J, McDermott HJ, Francart T. Sound Coding in Cochlear Implants: From electric pulses to hearing. *IEEE Signal Process Mag* 2015; 32:67–80.

[44] Franke-Trieger A, Jolly C, Darbinjan A, Zahnert T, Mürbe D. Insertion depth angles of cochlear implant arrays with varying length: a temporal bone study. *Otol Neurotol* 2014; 35:58–63.

[45] Adunka O, Kiefer J. Impact of electrode insertion depth on intracochlear trauma. *Otolaryngol Head Neck Surg* 2006; 135:374–382.

[46] Shannon RV, Cruz RJ, Galvin JJ. Effect of stimulation rate on cochlear implant users' phoneme, word and sentence recognition in quiet and in noise. *Audiol Neurotol* 2011; 16:113–123.

[47] Kiefer J, Von Ilberg C, Rupprecht V, Hubner-Egner J, Knecht R. Optimized speech understanding with the continuous interleaved sampling speech coding strategy in patients with cochlear implants: Effect of variations in stimulation rate and number of channels. *Ann Otol Rhinol Laryngol* 2000; 109:1009–1020.

[48] Wilson BS, Dorman MF. Cochlear implants: a remarkable past and a brilliant future. *Hear Res* 2008; 242:3–21.

[49] Doshi J, Johnson P, Mawman D, et al. Straight vs. modiolar hugging electrodes - does one perform better than the other? *Cochlear Implants Int* 2015; 16 Suppl 1:S33–35.

[50] Wolfe J, Schafer E. Programming Cochlear Implants. San Diego: Plural Publishing, 2015:23–24.

[51] Venail F, Mura T, Akkari M, et al. Modeling of Auditory Neuron Response Thresholds with Cochlear Implants. *Biomed Res Int* 2015; DOI: 10.1155/2015-394687.

[52] Fitzgerald MB, Shapiro WH, McDonald PD, et al. The effect of perimodiolar placement on speech perception and frequency discrimination by cochlear implant users. *Acta Otolaryngol* 2007; 127:378–383.

[53] Sanna M, Khrais T, Falcioni M, Russo A, Taibah A. The temporal bone. A manual for dissection and surgical approaches. Suttgart: Thieme, 2006:48–54.

[54] Gaylor JM, Raman G, Chung M, et al. Cochlear implantation in adults: a systematic review and meta-analysis. *JAMA Otolaryngol Head Neck Surg* 2013; 139:265–272.

[55] Van Schoonhoven J, Sparreboom M, Van Zanten BGA, et al. The effectiveness of bilateral cochlear implants for severe-to-profound deafness in children: a systematic review. *Otol Neurotol* 2010; 31:1062–1071.

[56] Senn P, Kompis M, Vischer M, Haeusler R. Minimum audible angle, just noticeable interaural differences and speech intelligibility with bilateral cochlear implants using clinical speech processors. *Audiol Neurotol* 2005; 10:342–352.

[57] Gstöttner W, Kiefer J, Baumgartner WD, Pok S, Peters S, Adunka O. Hearing preservation in cochlear implantation for electric acoustic stimulation. *Acta Otolaryngol* 2004; 124:348–352.

[58] Kiefer J, Gstöttner W, Baumgartner W, et al. Conservation of low-frequency hearing in cochlear implantation. *Acta Otolaryngol* 2004; 124:272–280.

[59] Gifford RH, Dorman MF, Skarzynski H, et al. Cochlear implantation with hearing preservation yields significant benefit for speech recognition in complex listening environments. *Ear Hear* 2013; 34:413–25.

[60] Irving S, Gillespie L, Richardson R, Rowe D, Fallon JB, Wise AK. Electroacoustic Stimulation: Now and into the Future. *Biomed Res Int* 2014; DOI: 10.1155/2014/350504.

[61] Causon A, Verschuur C, Newman TA. A Retrospective Analysis of the Contribution of Reported Factors in Cochlear Implantation on Hearing Preservation Outcomes. *Otol Neurotol* 2015; 36:1137–1145.

[62] Vlastarakos PV, Nazos K, Tavoulari EF, Nikolopoulos TP. Cochlear implantation for single-sided deafness: The outcomes. An evidence-based approach. *Eur Arch Otorhinolaryngol* 2014; 271:2119–2126.

[63] Tokita J, Dunn C, Hansen MR. Cochlear implantation and single-sided deafness. *Curr Opin Otolaryngol Head Neck Surg* 2014; DOI: 10.1097/MOO.0000000000000080.

[64] Blasco Ma, Redleaf MI. Cochlear Implantation in Unilateral Sudden Deafness Improves Tinnitus and Speech Comprehension: Meta-Analysis and Systematic Review. *Otol Neurotol* 2014; 35:1426–1432.

[65] Arts R, George EL, Stokroos RJ, Vermeire K. Review: cochlear implants as a treatment of tinnitus in single-sided deafness. *Curr Opin Otolaryngol Head Neck Surg* 2012; 20:398–403.

[66] Arts R, George EL, Griessner A, Zierhofer C, Stokroos RJ. Tinnitus Suppression by Intracochlear Electrical Stimulation in Single-Sided Deafness: A Prospective Clinical Trial - Part I. *Audiol Neurotol* 2015; 20:294–313.

[67] Kloostra FJ, Arnold R, Hofman R, Van Dijk P. Changes in Tinnitus after Cochlear Implantation and Its Relation with Psychological Functioning. *Audiol Neurotol* 2015; 20:81–89.

[68] Kompis M, Pelizzone M, Dillier N, Allum J, Demin N, Senn P. Tinnitus before and 6 months after cochlear implantation. *Audiol Neurotol* 2012; 17:161–168.

[69] Venail F, Sicard M, Piron JP, et al. Reliability and complications of 500 consecutive cochlear implantations. *Arch Otolaryngol Head Neck Surg* 2008; 134:1276–1281.

[70] Cosetti M, Roland Jr JT. Cochlear implant electrode insertion. *Oper Tech Otolaryngol* 2010; 21:223–232.

[71] House WF. Cochlear implants. *Ann Otol Rhinol Laryngol* 1976; 85:1–93.

[72] Aschendorff A, Gollner K, Maier W, et al. Technologisch-chirurgischer Fortschritt bei der Cochlear Implantation. Cochlear Implant Heute. Ed. by Ernst A, Battmer R, Todt I. Heidelberg: Springer Medizin Verlag, 2009:39–46.

[73] Bielamowicz SA, Coker NJ, Jenkins HA, Igarashi M. Surgical dimensions of the facial recess in adults and children. *Arch Otolaryngol Head Neck Surg* 1988; 114:534–537.

[74] Meshik X, Holden TA, Chole RA, Hullar TE. Optimal cochlear implant insertion vectors. *Otol Neurotol* 2010; 31:58–63.

[75] Zeitler DM, Balkany TJ. Alternative approaches to cochlear implantation. *Oper Tech Otolaryngol* 2010; 21:248–253.

[76] Dia A, Nogueira JF, O'Grady KM, Redleaf M. Report of endoscopic cochlear implantation. *Otol Neurotol* 2014; 35:1755–1758.

[77] Hiraumi H, Yamamoto N, Sakamoto T, Ito J. A minimally invasive approach for cochlear implantation using a microendoscope. *Eur Arch Otorhinolaryngol* 2013; 270:477–481.

[78] Marchioni D, Grammatica A, Alicandri-Ciufelli M, Genovese E, Presutti L. Endoscopic cochlear implant procedure. *Eur Arch Otorhinolaryngol* 2014; 271:959–966.

[79] Kronenberg J, Baumgartner W, Migirov L, Dagan T, Hildesheimer M. The suprameatal approach: an alternative surgical approach to cochlear implantation. *Otol Neurotol* 2004; 25:41–45.

[80] Arnoldner C, Gstoettner W, Riss D, et al. Residual hearing preservation using the suprameatal approach for cochlear implantation. *Wien Klin Wochenschr* 2011; 123:599–602.

[81] Kiratzidis T. 'Veria operation': cochlear implantation without a mastoidectomy and a posterior tympanotomy. A new surgical technique. *Adv Otorhinolaryngol* 2000; 57:127–130.

[82] Hans JM, Prasad R. Cochlear Implant Surgery by the Veria Technique: How and Why? Experience from 1400 Cases. *Indian J Otolaryngol Head Neck Surg* 2015; 67:107–109.

[83] Häusler R. Cochlear implantation without mastoidectomy: the pericanal electrode insertion technique. *Acta Otolaryngol* 2002; 122:715–719.

[84] Colletti V, Fiorino FG, Carner M, Pacini L. Basal turn cochleostomy via the middle fossa route for cochlear implant insertion. *Am J Otol* 1998; 19:778–784.

[85] Avci E, Nauwelaers T, Lenarz T, Hamacher V, Kral A. Variations in microanatomy of the human cochlea. *J Comp Neurol* 2014; 522:3245–3261.

[86] Zrunek M, Lischka M, Hochmair-Desoyer I, Burian K. Dimensions of the scala tympani in relation to the diameters of multichannel electrodes. *Arch Otorhinolaryngol* 1980; 229:159–165.

[87] Adunka OF, Radeloff A, Gstoettner WK, Pillsbury HC, Buchman C. Scala tympani cochleostomy II: topography and histology. *Laryngoscope* 2007; 117:2195–2200.

[88] Wanna GB, Noble JH, Carlson ML, et al. Impact of electrode design and surgical approach on scalar location and cochlear implant outcomes. *Laryngoscope* 2014; DOI: 10.1002/lary.24728.

[89] Holden LK, Finley CC, Firszt JB, et al. Factors affecting open-set word recognition in adults with cochlear implants. *Ear Hear* 2013; 34:342–360.

[90] Finley CC, Holden TA, Holden LK, et al. Role of electrode placement as a contributor to variability in cochlear implant outcomes. *Otol Neurotol* 2008; 29:920–928.

[91] Aschendorff A, Kromeier J, Klenzner T, Laszig R. Quality control after insertion of the nucleus contour and contour advance electrode in adults. *Ear Hear* 2007; 28:75S–79S.

[92] Adunka OF, Dillon MT, Adunka MC, King ER, Pillsbury HC, Buchman Ca. Cochleostomy versus round window insertions: influence on functional outcomes in electric-acoustic stimulation of the auditory system. *Otol Neurotol* 2014; 35:613–618.

[93] Havenith S, Lammers MJW, Tange Ra, et al. Hearing preservation surgery: cochleostomy or round window approach? A systematic review. *Otol Neurotol* 2013; 34:667–674.

[94] Gudis Da, Montes M, Bigelow DC, Ruckenstein MJ. The round window: is it the "cochleostomy" of choice? Experience in 130 consecutive cochlear implants. *Otol Neurotol* 2012; 33:1497–501.

[95] Skarzynski H, Lorens A, Zgoda M, Piotrowska A, Skarzynski PH, Szkielkowska A. Atraumatic round window deep insertion of cochlear electrodes. *Acta Otolaryngol* 2011; 131:740–749.

[96] Basura GJ, Adunka OF, Buchman Ca. Scala tympani cochleostomy for cochlear implantation. *Oper Tech Otolaryngol* 2010; 21:218–222.

[97] Berrettini S, Forli F, Passetti S. Preservation of residual hearing following cochlear implantation: comparison between three surgical techniques. *J Laryngol Otol* 2008; 122:246–252.

[98] Richard C, Fayad JN, Doherty J, Linthicum FH. Round Window Versus Cochleostomy Technique in Cochlear Implantation. *Otol Neurotol* 2012; 33:1181–1187.

[99] Roland PS, Wright CG, Isaacson B. Cochlear implant electrode insertion: the round window revisited. *Laryngoscope* 2007; 117:1397–1402.

[100] Briggs RJS, Tykocinski M, Stidham K, Roberson JB. Cochleostomy site: Implications for electrode placement and hearing preservation. *Acta Otolaryngol* 2005; 125:870–876.

[101] Skarzynski H, Podskarbi-Fayette R. A new cochlear implant electrode design for preservation of residual hearing: a temporal bone study. *Acta Otolaryngol* 2010; 130:435–442.

[102] Li PMMC, Wang H, Northrop C, Merchant SN, Nadol JB. Anatomy of the round window and hook region of the cochlea with implications for cochlear implantation and other endocochlear surgical procedures. *Otol Neurotol* 2007; 28:641–648.

[103] Marel KS van der, Briaire JJ, Verbist BM, Muurling TJ, Frijns JHM. The influence of cochlear implant electrode position on performance. *Audiol Neurotol* 2015; 20:202–211.

[104] Buchman CA, Dillon MT, King ER, Adunka MC, Adunka OF, Pillsbury HC. Influence of Cochlear Implant Insertion Depth on Performance. *Otol Neurotol* 2014; 35:1773–1779.

[105] Lee J, Nadol JB, Eddington DK. Depth of electrode insertion and postoperative performance in humans with cochlear implants: A histopathologic study. *Audiol Neurotol* 2010; 15:323–331.

[106] Yukawa K, Cohen L, Blamey P, Pyman B, Tungvachirakul V, O'Leary S. Effects of insertion depth of cochlear implant electrodes upon speech perception. *Audiol Neurotol* 2004; 9:163–172.

[107] Skinner MW, Ketten DR, Holden LK, et al. CT-derived estimation of cochlear morphology and electrode array position in relation to word recognition in nucleus-22 recipients. *J Assoc Res Otolaryngol* 2002; 3:332–350.

[108] Landsberger DM, Svrakic M, Roland JT, Svirsky M. The Relationship Between Insertion Angles, Default Frequency Allocations, and Spiral Ganglion Place Pitch in Cochlear Implants. *Ear Hear2* 2015; 36:207–213.

[109] Venail F, Mathiolon C, Menjot de Champfleur S, et al. Effects of Electrode Array Length on Frequency-Place Mismatch and Speech Perception with Cochlear Implants. *Audiol Neurotol* 2015; 2:102–111.

[110] Schipper J, Aschendorff A, Arapakis I, et al. Navigation as a quality management tool in cochlear implant surgery. *J Laryngol Otol* 2004; 118:764–770.

[111] Labadie RF, Chodhury P, Cetinkaya E, et al. Minimally invasive, image-guided, facial-recess approach to the middle ear: demonstration of the concept of percutaneous cochlear access in vitro. *Otol Neurotol* 2005; 26:557–562.

[112] Labadie RF, Balachandran R, Noble JH, et al. Minimally invasive image-guided cochlear implantation surgery: First report of clinical implementation. *Laryngoscope* 2014; 124:1915–1922.

[113] Klenzner T, Ngan C, Knapp F, Knoop H, Kromeier J, Aschendorff A. New strategies for high precision surgery of the temporal bone using a robotic approach for cochlear implantation. *Eur Arch Otorhinolaryngol* 2009; 266:955–960.

[114] Baron S, Eilers H, Munske B, et al. Percutaneous inner-ear access via an image-guided industrial robot system. *Proc Inst Mech Eng H* 2010; 224:633–649.

[115] Kobler JP, Kotlarski J, Oltjen J, Baron S, Ortmaier T. Design and analysis of a head-mounted parallel kinematic device for skull surgery. *Int J Comput Assist Radiol Surg* 2012; 7:137–149.

[116] Kratchman LB, Blachon GS, Withrow TJ, Balachandran R, Labadie RF, Webster RJ. Design of a bone-attached parallel robot for percutaneous cochlear implantation. *IEEE Trans Biomed Eng* 2011; 58:2904–2910.

[117] Stieger C, Caversaccio M, Arnold A, et al. Development of an auditory implant manipulator for minimally invasive surgical insertion of implantable hearing devices. *J Laryngol Otol* 2011; 125:262–270.

[118] Bell B, Gerber N, Williamson T, et al. In vitro accuracy evaluation of image-guided robot system for direct cochlear access. *Otol Neurotol* 2013; 34:1284–1290.

[119] Gerber N, Bell B, Gavaghan K, Weisstanner C, Caversaccio M, Weber S. Surgical planning tool for robotically assisted hearing aid implantation. *Int J Comput Assist Radiol Surg* 2014; 9:11–20.

[120] Gerber N, Gavaghan K, Bell B, et al. High accuracy patient-to-image registration for the facilitation of image-guided robotic microsurgery on the head. *IEEE Trans Biomed Eng* 2013; 60:960–968.

[121] Williamson TM, Bell BJ, Gerber N, et al. Estimation of tool pose based on force-density correlation during robotic drilling. *IEEE Trans Biomed Eng* 2013; 60:969–976.

[122] Ansó J, Stahl C, Gerber N, et al. Feasibility of Using EMG for Early Detection of the Facial Nerve During Robotic Direct Cochlear Access. *Otol Neurotol* 2014; 35:545–554.

[123] Vaerenberg B, Smits C, De Ceulaer G, et al. Cochlear Implant Programming: A Global Survey on the State of the Art. *ScientificWorldJournal* 2014; DOI: 10.1155/2014/501738.

[124] Drennan WR, Oleson JJ, Gfeller K, et al. Clinical evaluation of music perception, appraisal and experience in cochlear implant users. *Int J Audiol* 2014; 54:114–123.

[125] Hinderink JB, Krabbe PF, Van Den Broek P. Development and application of a health-related quality-of-life instrument for adults with cochlear implants: the Nijmegen cochlear implant questionnaire. *Otolaryngol Head Neck Surg* 2000; 123:756–765.

[126] Robinson K, Gatehouse S, Browning GG. Measuring patient benefit from otorhinolaryngological surgery and therapy. *Ann Otol Rhinol Laryngol* 1996; 105:415–422.

[127] Newman CW, Jacobson GP, Spitzer JB. Development of the Tinnitus Handicap Inventory. *Arch Otolaryngol Head Neck Surg* 1996; 122:143–148.

[128] Kompis M, Bettler M, Vischer M, Senn P, Häusler R. Bilateral cochlear implantation and directional multi-microphone systems. *International Congress Series* 2004; 1273:447–450.

[129] Moberly AC, Lowenstein JH, Nittrouer S. Word Recognition Variability With Cochlear Implants: "Perceptual Attention" Versus "Auditory Sensitivity". *Ear Hear* 2015; in press.

[130] Lazard DS, Vincent C, Venail F, et al. Pre-, Per- and Postoperative Factors Affecting Performance of Postlinguistically Deaf Adults Using Cochlear Implants: A New Conceptual Model over Time. *PLoS ONE* 2012; DOI: 10.1371/journal.pone.0048739. Ed. by Malmierca MS.

[131] Bhatti P, Van Beek-King J, Sharpe A, et al. Highly Flexible Silicone Coated Neural Array for Intracochlear Electrical Stimulation. *Biomed Res Int* 2015; DOI: 10.1155/2015/109702.

[132] Alexiades G, Dhanasingh A, Jolly C. Method to Estimate the Complete and Two-Turn Cochlear Duct Length. *Otol Neurotol* 2015; 36:904–907.

[133] Nguyen Y, Kazmitcheff G, De Seta D, Miroir M, Ferrary E, Sterkers O. Definition of Metrics to Evaluate Cochlear Array Insertion Forces Performed with Forceps, Insertion Tool, or Motorized Tool in Temporal Bone Specimens. *Biomed Res Int* 2014; DOI: 10.1155/2014/532570.

[134] El Kechai N, Agnely F, Mamelle E, Nguyen Y, Ferrary E, Bochot A. Recent advances in local drug delivery to the inner ear. *Int J Pharm* 2015; 494:83–101.

[135] Staecker H, Jolly C, Garnham C. Cochlear implantation: an opportunity for drug development. *Drug Discov Today* 2010; 15:314–321.

[136] Mauger S, Warren C, Knight M, Goorevich M, Nel E. Clinical evaluation of the Nucleus 6 cochlear implant system: performance improvements with SmartSound iQ. *Int J Audiol* 2014; 53:564–76.

[137] Skarzynski H, Lorens A, Piotrowska A, Anderson I. Preservation of low frequency hearing in partial deafness cochlear implantation (PDCI) using the round window surgical approach. *Acta Otolaryngol* 2007; 127:41–48.

[138] Adunka O, Gstoettner W, Hambek M, Unkelbach MH, Radeloff A, Kiefer J. Preservation of basal inner ear structures in cochlear implantation. *ORL J Otorhinolaryngol Relat Spec* 2004; 66:306–12.

[139] Tóth M, Alpár A, Patonay L, Oláh I. Development and surgical anatomy of the round window niche. *Ann Anat* 2006; 188:93–101.

[140] Majdani O, Bartling SH, Leinung M, et al. Image-guided minimal-invasive cochlear implantation - experiments on cadavers (in German). *Laryngorhinootologie* 2008; 87:18–22.

[141] Schipper J, Klenzner T, Aschendorff A, Arapakis I, Ridder GJ, Laszig R. Navigation-controlled cochleostomy. Is an improvement in the quality of results for cochlear implant surgery possible? (in German). *HNO* 2004; 52:329–335.

[142] Verbist BM, Skinner MW, Cohen LT, et al. Consensus panel on a cochlear coordinate system applicable in histologic, physiologic, and radiologic studies of the human cochlea. *Otol Neurotol* 2010; 31:722–730.

[143] Möller T, Trumbore B. Fast, minimum storage ray/triangle intersection. Journal of Graphics Tools. ACM. 2005:21–28.

[144] Wimmer W, Bell B, Huth ME, et al. Cone beam and micro-computed tomography validation of manual array insertion for minimally invasive cochlear implantation. *Audiol Neurotol* 2014; 19:22–30.

[145] Gantz BJ, Turner C, Gfeller KE, Lowder MW. Preservation of hearing in cochlear implant surgery: advantages of combined electrical and acoustical speech processing. *Laryngoscope* 2005; 115:796–802.

[146] Balachandran R, Mitchell JE, Blachon G, et al. Percutaneous cochlear implant drilling via customized frames: an in vitro study. *Otolaryngol Head Neck Surg* 2010; 142:421–426.

[147] Labadie RF, Noble JH, Dawant BM, Balachandran R, Majdani O, Fitzpatrick JM. Clinical validation of percutaneous cochlear implant surgery: initial report. *Laryngoscope* 2008; 118:1031–1039.

[148] Hussong A, Rau TS, Ortmaier T, Heimann B, Lenarz T, Majdani O. An automated insertion tool for cochlear implants: another step towards atraumatic cochlear implant surgery. *Int J Comput Assist Radiol Surg* 2010; 5:163–171.

[149] Kratchman LB, Schurzig D, McRackan TR, et al. A manually operated, advance off-stylet insertion tool for minimally invasive cochlear implantation surgery. *IEEE Trans Biomed Eng* 2012; 59:2792–2800.

[150] Thiel W. The preservation of the whole corpse with natural color (in German). *Ann Anat* 1992; 174:185–195.

[151] Xu J, Xu S, Cohen L, Clark G. Cochlear view: postoperative radiography for cochlear implantation. *Am J Otol* 2000; 21:49–56.

[152] Eshraghi A, Yang N, Balkany T. Comparative study of cochlear damage with three perimodiolar electrode designs. *Laryngoscope* 2003; 113:415–419.

[153] Alberty J, Filler T, Schmäl F, Peuker E. Thiel method fixed cadaver ears: a new procedure for graduate and continuing education in middle ear surgery (in German). *HNO* 2002; 50:739–742.

[154] Benkhadra M, Gérard J, Genelot D, et al. Is Thiel's embalming method widely known? A world survey about its use. *Surg Radiol Anat* 2011; 33:359–363.

[155] Cushing SL, Daly MJ, Treaba CG, et al. High-resolution cone-beam computed tomography: a potential tool to improve atraumatic electrode design and position. *Acta Otolaryngol* 2012; 132:361–368.

[156] Kurzweg T, Dalchow CV, Bremke M, et al. The value of digital volume tomography in assessing the position of cochlear implant arrays in temporal bone specimens. *Ear Hear* 2010; 31:413–419.

[157] Güldner C, Wiegand S, Weiss R, et al. Artifacts of the electrode in cochlea implantation and limits in analysis of deep insertion in cone beam tomography (CBT). *Eur Arch Otorhinolaryngol* 2012; 269:767–772.

[158] Teymouri J, Hullar T, Holden T, Chole R. Verification of computed tomographic estimates of cochlear implant array position: a micro-CT and histological analysis. *Otol Neurotol* 2011; 32:980–986.

[159] Stenfelt S. Bilateral fitting of BAHAs and BAHA fitted in unilateral deaf persons: acoustical aspects. *Int J Audiol* 2005; 44:178–189.

[160] Pfiffner F, Caversaccio MD, Kompis M. Comparisons of sound processors based on osseointegrated implants in patients with conductive or mixed hearing loss. *Otol Neurotol* 2011; 32:728–735.

[161] Kompis M, Krebs M, Häusler R. Verification of normative values for the Swiss version of the Freiburg speech intelligibility test (in German). *HNO* 2006; 54:445–450.

[162] Wagener K, Brand T, Kollmeier B. Development and evaluation of a German sentence test part II: evaluation of the Oldenburg sentence test (in German). *Audiol Acoust* 1999; 38:86–95.

[163] Greenberg JE, Peterson PM, Zurek PM. Intelligibility-weighted measures of speech-to-interference ratio and speech system performance. *J Acoust Soc Am* 1993; 94:3009–3010.

[164] ANSI S3.5-1997. Methods for calculation of the speech intelligibility index. New York: American National Standards Institute, 1997.

[165] Kompis M, Dillier N. Simulating transfer functions in a reverberant room including source directivity and head-shadow effects. *J Acoust Soc Am* 1993; 93:2779–2787.

[166] Schwarz L. On the theory of diffraction of a plane soundwave around a sphere (in German). *Akust Z* 1943; 8:91–117.

[167] Kuhn G. Model for the interaural time differences in the azimuthal plane. *J Acoust Soc Am* 1977; 62:157–167.

[168] Mertens G, Hofkens A, Punte AK, De Bodt M, Van de Heyning P. Hearing performance in single-sided deaf cochlear implant users after upgrade to a single-unit speech processor. *Otol Neurotol* 2015; 36:51–60.

[169] Büchner A, Dyballa KH, Hehrmann P, Fredelake S, Lenarz T. Advanced beamformers for cochlear implant users: Acute measurement of speech perception in challenging listening conditions. *PLoS ONE* 2014; DOI: 10.1371/journal.pone.-0095542.

[170] Goldsworthy RL. Two-microphone spatial filtering improves speech reception for cochlear-implant users in reverberant conditions with multiple noise sources. *Trends Hear* 2014; DOI: 10.1177/2331216514555489.

[171] Kompis M, Bertram M, Senn P, Müller J, Pelizzone M, Häusler R. A two-microphone noise reduction system for cochlear implant users with nearby microphones - part II: performance evaluation. *Eurasip J Adv Sig Pr* 2008; DOI: 10.1155/2008/451273.

[172] Spriet A, Van Deun L, Eftaxiadis K, et al. Speech understanding in background noise with the two-microphone adaptive beamformer BEAM in the Nucleus Freedom cochlear implant system. *Ear Hear* 2007; 28:62–72.

[173] Van den Bogaert T, Carette E, Wouters J. Sound source localization using hearing aids with microphones placed behind-the-ear, in-the-canal, and in-the-pinna. *Int J Audiol* 2011; 50:164–176.

[174] Olze H, Gräbel S, Haupt H, Förster U, Mazurek B. Extra benefit of a second cochlear implant with respect to health-related quality of life and tinnitus. *Otol Neurotol* 2012; 33:1169–1175.

[175] Hey M, Hocke T, Hedderich J, Müller-Deile J. Investigation of a matrix sentence test in noise: reproducibility and discrimination function in cochlear implant patients. *Int J Audiol* 2014; 53:895–902.

[176] Rader T. Speech perception with electric-acoustic stimulation: Comparison with bilateral cochlear implant users in different noise conditions (in German). *HNO* 2015; 63:85–93.

[177] Wolfe J, Schafer EC, Heldner B, Mülder H, Ward E, Vincent B. Evaluation of speech recognition in noise with cochlear implants and dynamic FM. *J Am Acad Audiol* 2009; 20:409–421.

[178] Nelson PB, Jin SH, Carney AE, Nelson DA. Understanding speech in modulated interference: cochlear implant users and normal-hearing listeners. *J Acoust Soc Am* 2003; 113:961–968.

[179] Wolfe J, Parkinson A, Schafer EC, et al. Benefit of a commercially available cochlear implant processor with dual-microphone beamforming. *Otol Neurotol* 2012; 33:553–560.

[180] Gifford RH, Revit LJ. Speech perception for adult cochlear implant recipients in a realistic background noise: effectiveness of preprocessing strategies and external options for improving speech recognition in noise. *J Am Acad Audiol* 2010; 21:441–451.

[181] Chung K, Zeng FG. Using hearing aid adaptive directional microphones to enhance cochlear implant performance. *Hear Res* 2009; 250:27–37.

[182] Chung K, Zeng FG, Acker KN. Effects of directional microphone and adaptive multichannel noise reduction algorithm on cochlear implant performance. *J Acoust Soc Am* 2006; 120:2216–2227.

[183] Brockmeyer AM, Potts LG. Evaluation of different signal processing options in unilateral and bilateral cochlear freedom implant recipients using R-Space background noise. *J Am Acad Audiol* 2011; 22:65–80.

[184] Wouters J, Vanden Berghe J. Speech recognition in noise for cochlear implantees with a two-microphone monaural adaptive noise reduction system. *Ear Hear* 2001; 22:420–430.

[185] Kuk F, Korhonen P, Lau C, Keenan D, Norgaard M. Evaluation of a pinna compensation algorithm for sound localization and speech perception in noise. *Am J Audiol* 2013; 22:84–93.

[186] Kayser H, Ewert SD, Anemüller J, Rohdenburg T, Hohmann V, Kollmeier B. Database of multichannel in-ear and behind-the-ear head-related and binaural room impulse responses. *Eurasip J Adv Sig Pr* 2009; DOI: 10.1155/2009/298605.

[187] Wimmer W, Caversaccio M, Kompis M. Speech intelligibility in noise with a single-unit cochlear implant audio processor. *Otol Neurotol* 2015; 36:1197–1202.

[188] Williamson T, Du X, Bell B, et al. Mechatronic feasibility of minimally invasive, atraumatic cochleostomy. *Biomed Res Int* 2014; DOI: 10.1155/2014/181624.

CURRICULUM VITAE

Wimmer, Wilhelm

Personal Information

Date of birth	October 22nd 1985
Place of birth	Tizi Ouzou, Algeria
Nationality	Austrian

Education

2012 - 2015	Ph.D. in Biomedical Engineering, Artificial Hearing Research ARTORG Center for Biomedical Engineering Research University of Bern, Switzerland Thesis: *Multidisciplinary Approaches toward an Improved Efficacy of Cochlear Implants*
2010 - 2012	M.Sc. in Biomedical Engineering, Institute of Medical Engineering Graz University of Technology, Austria Thesis: *Multispeaker Setup for Audiological Measurements using Gesture Recognition*
2006 - 2010	B.Sc. in Biomedical Engineering, Institute of Medical Engineering Graz University of Technology, Austria Thesis: *Konstruktion eines beheizten Tierbetts für MR-Untersuchungen*
2000 - 2005	Technical college degree in Structural Engineering, HTL 1 Linz, Austria

Professional Experience

2012	Research assistant,Institute of Medical Engineering Graz University of Technology, Austria
2009 - 2012	Technical project engineer, dp Projektform AG Graz, Austria
2007 - 2010	Audio engineer, Haus der Architektur Graz, Austria

LIST OF PUBLICATIONS

Journal Articles

Wimmer W, Weder S, Caversaccio M, Kompis M. Speech intelligibility in noise with a pinna effect imitating cochlear implant processor. *Otol Neurotol* 2016; 37:19-23.

Wagner F, **Wimmer W**, Leidolt L, Vischer M, Weder S, Wiest R, Mantokoudis J, Caversaccio M. Significant artifact reduction at 1.5T and 3T MRI by the use of a cochlear implant with removable magnet: an experimental human cadaver study. *PloS One* 2015; DOI: 10.1371/journal.pone.0132483.

Wimmer W, Caversaccio M, Kompis M. Speech intelligibility in noise with a single-unit cochlear implant audio processor. *Otol Neurotol* 2015; 36:1197-1202.

Venail F, Bell B, Akkari M, **Wimmer W**, Williamson T, Gerber N, Gavaghan K, Canovas F, Weber S, Caversaccio M, Uziel A. Manual electrode array insertion through a robot-assisted minimal invasive cochleostomy: feasibility and comparison of two different electrode array subtypes. *Otol Neurotol* 2015; 36:1015-1022.

Wimmer W, Gerber N, Guignard J, Dubach P, Kompis M, Weber S, Caversaccio M. Topographic bone thickness maps for Bonebridge implantations. *Eur Arch Otorhinolaryngol* 2015; 272:1651-1658.

Wimmer W, Venail F, Williamson T, Akkari M, Gerber N, Weber S, Caversaccio M, Uziel A, Bell B. Semiautomatic cochleostomy target and insertion trajectory planning for minimally invasive cochlear implantation. *Biomed Res Int* 2014; DOI: 10.1155/2014/596498.

Wimmer W, Bell B, Huth ME, Weisstanner C, Gerber N, Kompis M, Weber S, Caversaccio M. Cone beam and micro-computed tomography validation of manual array insertion for minimally invasive cochlear implantation. *Audiol Neurotol* 2014; 19:22-30.

Bell B, Gerber N, Williamson T, Gavaghan K, **Wimmer W**, Caversaccio M, Weber S. In vitro accuracy evaluation of image-guided robot system for direct cochlear access. *Otol Neurotol* 2013; 34:1284-1290.

Conference Papers and Abstracts

Wimmer W, Caversaccio M, Kompis M. Sprachverstehen im Störlärm mit dem Sonnet CI Sprachprozessor. *Herbsttagung ADANO*, Bern, Switzerland 2015.

Barakchieva M, **Wimmer W**, Dubach P, Arnold A, Caversaccio M, Gerber N. Surgical planning tool for Bonebridge implantation using topographic bone thickness maps. *Computer Assisted Radiology and Surgery, 29th international congress and exhibition*, Barcelona, Spain 2015.

Wimmer W, Caversaccio M, Kompis M. Sprachverstehen im Störlärm mit dem Sonnet CI Sprachprozessor. *18. Jahrestagung Deutsche Gesellschaft für Audiologie*, Bochum, Germany 2015.

Dubach P, Hofer M, **Wimmer W**, Dietz A, Mozet C, Gerber N, Kompis M, Weber S, Caversaccio M. Klinische Evaluation der Knochendickenkartographie zur Planung der Bonebridge Implantation – eine Schweizerisch-Deutsche Kooperation. *85. Jahresversammlung der DGHNO KHC*, Dortmund, Germany 2014.

Venail F, Bell B, Akkari M, **Wimmer W**, Williamson T, Weber S. Implantation cochléaire par cochléostomie minimale invasive robot assistée: faisabilité et comparaison de 2 faisceaux d'électrodes. *121e congrès annuel de la société Française de l'ORL*, Paris, France 2014.

Kompis M, **Wimmer W**, Caversaccio M. Speech understanding in noise with the Medel Opus 2 and Rondo sound processors. *14th Symposium on Cochlear Implants in Children*, Nashville, USA 2014.

Venail F, **Wimmer W**, Akkari M, Williamson T, Gerber N, Uziel A, Weber S, Bell B. Image-guided and robot-assisted cochleostomy for cochlear implantation: a feasibility study. *13th International Conference on Cochlear Implants and other Implantable Auditory Technologies*, Munich, Germany 2014.

Wimmer W, Gerber N, Bell B, Dhanasingh A, Jolly S, Weber S, Kompis M, Caversaccio M. Cochlear duct length estimation: adaptation of Escude's equation. *13th International Conference on Cochlear Implants and other Implantable Auditory Technologies*, Munich, Germany 2014.

Dhanasingh A, Jolly C, Mistrik P, **Wimmer W**, Kompis M, Caversaccio M. Complete Cochlear Coverage - Importance and method to achieve it. *13th International Conference on Cochlear Implants and other Implantable Auditory Technologies*, Munich, Germany 2014.

Senn P, Schmid C, Wieland T, Vischer M, **Wimmer W**, Mantokoudis G, Caversaccio M, Kompis M. Cochlear Implantation After 5 To 50 Years Of Deafness. *13th International Conference on Cochlear Implants and other Implantable Auditory Technologies*, Munich, Germany 2014.

Bell B, Williamson T, Gerber N, Gavaghan K, **Wimmer W**, Kompis M, Weber S, Caversaccio M. An image-guided robot system for direct cochlear access. In: *Cochlear Implants Int* 2014; 15 Suppl 1:11-13.

Weber S, Gerber N, Gavaghan K, Williamson T, **Wimmer W**, Anso J, Brogna-Salas L, Chen D, Weisstanner C, Caversaccio M, Bell B. Image guided and robotic assisted minimally invasive cochlear implantation. *Hamlyn Symposium on Medical Robotics*, London, United Kingdom 2013.

Wimmer W, Gerber N, Dhanasingh A, Mistrik P, Jolly C, Bell B, Weber S, Kompis M, Caversaccio M. In vitro micro-CT validation of preoperative cochlear duct length estimation. In: *Proceedings of the annual meeting of the German Society for Computer and Robot Assisted Surgery*, Innsbruck, Austria 2013; 143-146.

Wimmer W, Guignard J, Gerber N, Kompis M, Weber S, Caversaccio M. A preoperative planning method for Bonebridge implantations using surface distance maps. *Computer Assisted Radiology and Surgery, 27th international congress and exhibition*, Heidelberg, Germany 2013.

Wimmer W, Guignard J, Gerber N, Weber S, Häusler R, Kompis M, Caversaccio M. Bonebridge: Präoperative Planungsmethode und erste Erfahrungen. *100. Frühjahrsversammlung der Schweizerischen Gesellschaft für Oto-Rhino-Laryngologie, Hals- und Gesichtschirurgie*, Zermatt, Switzerland 2013.

DECLARATION OF ORIGINALITY

Last name, first name: Wimmer, Wilhelm

Matriculation number: 12-137-485

I hereby declare that this thesis represents my original work and that I have used no other sources except as noted by citations.
All data, tables, figures and text citations which have been reproduced from any other source, including the internet, have been explicitly acknowledged as such.
I am aware that in case of non-compliance, the Senate is entitled to withdraw the doctorate degree awarded to me on the basis of the present thesis, in accordance with the "Statut der Universität Bern (Universitätsstatut; UniSt)", Art. 69, of 7 June 2011.

Bern, December 11th 2015

Place, date

Signature